Palaeogeography, Palaeoclimatology, Palaeoecology 625 (2023) 111669

Contents lists available at ScienceDirect

Palaeogeography, Palaeoclimatology, Palaeoecology

journal homepage: www.elsevier.com/locate/palaeo

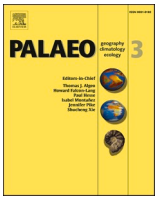

The Lutetian global stratotype section and point at Gorrondatxe revisited: Biomagnetostratigraphic refinements and astronomical tuning

Aitor Payros [a,*], Naroa Martínez-Braceras [a,b], Jaume Dinarès-Turell [c], Gilen Bernaola [d], Simonetta Monechi [e]

[a] Department of Geology, Faculty of Science and Technology, University of the Basque Country (UPV/EHU), Ap. 644, E-48080 Bilbao, Spain
[b] Laboratorio de Evolución Humana, Departamento de Historia, Geografía y Comunicación, Universidad de Burgos, Edificio I+D+I, Plaza de Misael Bañuelos s/n, 09001 Burgos, Spain
[c] Istituto Nazionale di Geofisica e Vulcanologia, Via di Vigna Murata 605, I-00142 Roma, Italy
[d] Department of Mining and Metallurgical Engineering, Bilbao School of Engineering, University of the Basque Country (UPV/EHU), Plaza Ingeniero Torres Quevedo 1, E-48013 Bilbao, Spain
[e] Università Degli Studi di Firenze, via La Pira 4, I-50121 Firenze, Italy

ARTICLE INFO

Editor: M Elliot

Keywords:
Ypresian/Lutetian boundary
Eocene
Hemipelagic deposit
Magnetostratigraphy
Calcareous nannofossil biostratigraphy
Cyclostratigraphy

ABSTRACT

Biomagnetostratigraphic studies carried out at the Ypresian/Lutetian (Eocene) Gorrondatxe section solved major chronostratigraphic calibration discrepancies that had existed for several decades. The new calibration resulted in the definition of the Global Stratotype Section and Point (GSSP) for the Lutetian Stage at the Gorrondatxe layer containing the lowest occurrence (LO) of the calcareous nannofossil *Blackites inflatus* (base of Subzone CP12b). However, subsequent studies cast some doubt on the reliability of the Gorrondatxe biomagnetostratigraphic data and, consequently, the appropriateness of the criterion used for the definition of the Lutetian GSSP. In order to address the issues raised, the biomagnetostratigraphy of the Gorrondatxe section was revisited and an additional cyclostratigraphic analysis was undertaken using magnetic susceptibility data series. The present study shows that the Gorrondatxe biomagnetostratigraphy is reliable. The spectral analyses showed the dominance of precession (~20 ky) and short (~100 ky) eccentricity forcing on sedimentation, but the influence of obliquity (~38 and ~ 55 ky) cycles was also detected and modulation by long (405 ky) eccentricity cycles was deduced. The succession was tuned to the 49.122–48.084 Ma interval and the astronomical ages obtained for a significant number of biomagnetostratigraphic events compared well with those derived from other studies. One of the exceptions is the LO of *B. inflatus*, which seems to be older in Gorrondatxe than in the Mediterranean and Western Atlantic areas. This diachrony most likely also delayed the LO of *B. inflatus* in historical reference sections of the North Sea area, rendering previous claims that the Lutetian GSSP caused some historical Lutetian sections to be Ypresian in age invalid. In fact, the definition of the base of the Lutetian Stage by the LO of *B. inflatus* at Gorrondatxe, now astronomically age dated at 48.455 Ma, best guarantees that the original concepts of the Ypresian and Lutetian historical stratotypes are maintained. Combined with secondary biomagnetostratigraphic marker events and an astronomically tuned cyclostratigraphy, the Ypresian/Lutetian Gorrondatxe section provides the globally significant chronostratigraphic reference model expected of any GSSP.

1. Introduction

The Ypresian and Lutetian are the oldest standard stages of the Eocene Epoch at a global scale (see Speijer et al., 2020 for a recent update). The Ypresian was originally defined in clayey and sandy shelfal deposits found in Belgium, whereas the Lutetian was defined in the Paris Basin to refer to shallow-marine carbonate deposits (Molina et al., 2011). A stratigraphic gap occurs between both units, which includes the Ypresian/Lutetian boundary.

The calibration between Ypresian–Lutetian biostratigraphic and magnetostratigraphic timescales varied considerably over several decades (see references in Payros et al., 2007). More recently, following

* Corresponding author.
E-mail addresses: a.payros@ehu.eus (A. Payros), naroa.martinez@ehu.eus (N. Martínez-Braceras), jaume.dinares@ingv.it (J. Dinarès-Turell), gilen.bernaola@ehu.eus (G. Bernaola), simonetta.monechi@unifi.it (S. Monechi).

https://doi.org/10.1016/j.palaeo.2023.111669
Received 1 December 2022; Received in revised form 4 April 2023; Accepted 4 June 2023
Available online 16 June 2023

the advent of astronomical timescales, the Ypresian–Lutetian interval was found to be difficult to complete from a cyclostratigraphic point of view (Hilgen et al., 2010; Westerhold et al., 2015). The difficulty in establishing reliable Ypresian–Lutetian timescales was a consequence of the scarcity of continuous sections with a good biomagnetostratigraphic record. This problem was partly solved with the study of the Gorrondatxe section (Basque Country, western Pyrenees; Lat. 43°23′N, Long. 3°01′W; Fig. 1A). This continuous and expanded succession allowed the precise calibration of several biostratigraphic and magnetostratigraphic events around the Ypresian–Lutetian transition, but resulted in a

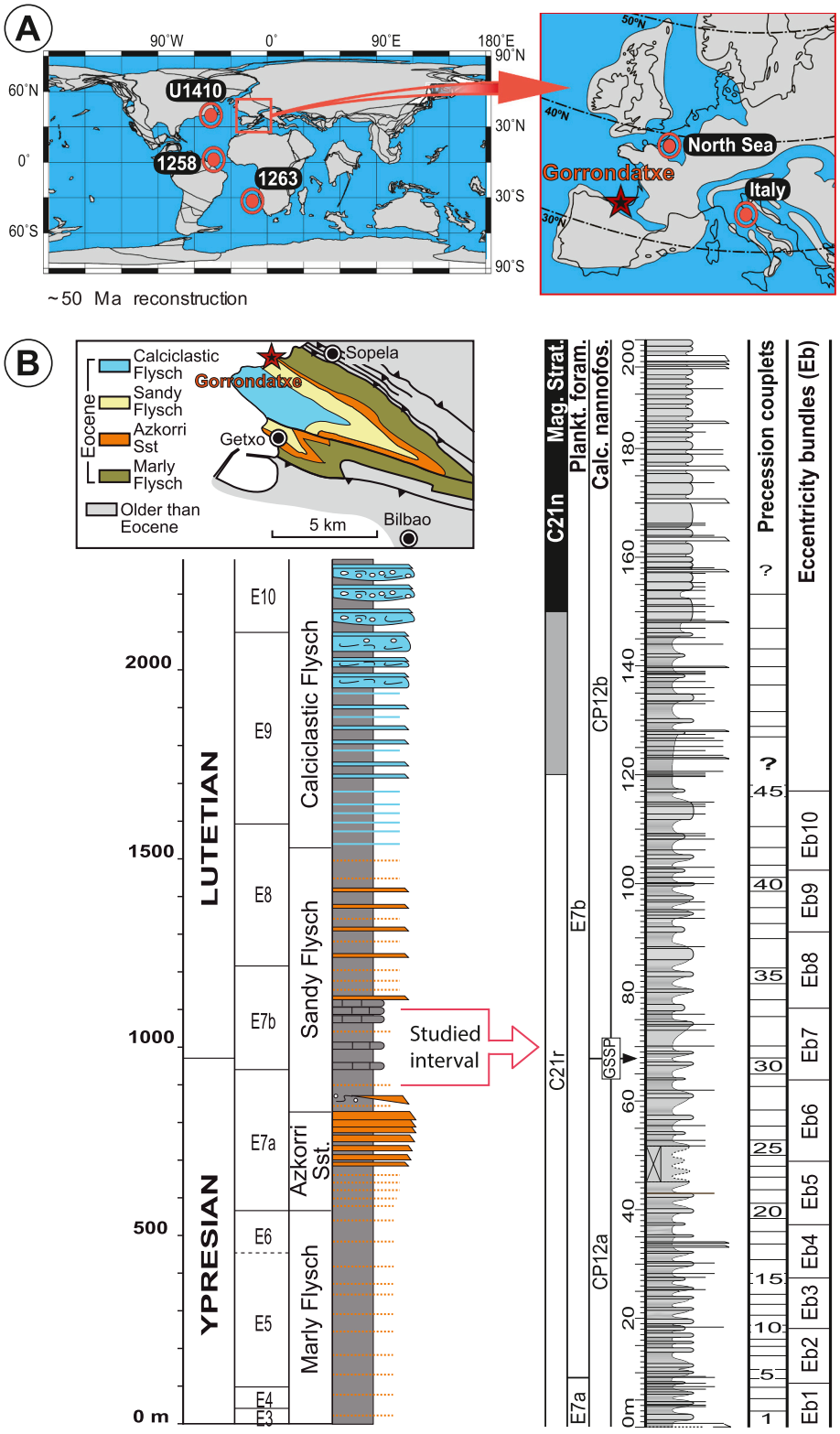

Fig. 1. (A) Location of Gorrondatxe (Lutetian GSSP) and other sections mentioned in the text on a 50 Ma paleogeographic reconstruction (from http://www.odsn.de). (B) Geological map and stratigraphic log of the Eocene deposits in the Gorrondatxe area, with an enlargement for the Ypresian/Lutetian interval studied herein. The position of the Lutetian GSSP is shown (for chronostratigraphic details, see Molina et al., 2011).

correlation framework that was at odds with all previous timescales by approximately 3 My (Bernaola et al., 2006; Payros et al., 2007, 2009, 2011). Despite the initial reluctance of the scientific community to accept the alternative chronostratigraphic calibration, subsequent independent studies from other areas confirmed the Gorrondatxe framework. This led to the amendment of the standard chronostratigraphic scale and the development of the revised version that stands to date (Wade et al., 2011; Vandenberghe et al., 2012; Speijer et al., 2020). The acceptance of this alternative chronostratigraphic framework eventually resulted in the definition of the Global Stratotype Section and Point (GSSP) for the base of the Lutetian Stage at the marl bed that records the lowest occurrence (LO) of the calcareous nannofossil *Blackites inflatus* (base of Subzone CP12b) at the Gorrondatxe section (Molina et al., 2011; Fig. 1B; supplementary Fig. S1). This level occurs in an interval attributed to the lower part of planktonic foraminiferal Zone E7b and the middle part of magnetic polarity Chron C21r (C21r.6 according to Vandenberghe et al., 2012). Based on the number of limestone-marl couplets between magnetic polarity reversals and the GSSP level, which were attributed to astronomical precession cycles of ca. 20 ky (Payros et al., 2009, 2011), the base of the Lutetian Stage at Gorrondatxe was age dated at 47.76 Ma (relative to Luterbacher et al., 2004; subsequently rounded at 47.80 Ma in Vandenberghe et al., 2012, and established at 48.07 Ma in Speijer et al., 2020).

However, several recent studies have put in doubt the reliability of the Gorrondatxe biomagnetostratigraphic data, the appropriateness of the criterion used for the definition of the Lutetian GSSP, and its absolute age as derived from Gorrondatxe. More specifically, several studies carried out in other areas found the LO of *B. inflatus* in a higher position, near the C21r/C21n chron reversal or within Chron C21n (Norris et al., 2014; Franceschi et al., 2015; Westerhold et al., 2017; Cappelli et al., 2019), casting doubt on the reliability of the magnetostratigraphy from Gorrondatxe. Alternatively, these studies acknowledged that the discrepancy could have arisen from a diachrony in the global LO of *B. inflatus*, as this species was more common in relatively shallow waters than in true pelagic settings, which would argue against the appropriateness of this bioevent being considered a global chronostratigraphic marker. In this regard, Steurbaut and Nolf (2021) also reported that *B. inflatus* is very rare in Eocene successions from the North Sea area, including the historical Lutetian stratotype in the Paris Basin. More importantly, they showed that this species is absent from reference Lutetian deposits in the North Sea area, but some successions contain a newly defined precursor species, namely *Blackites praeinflatus*. As a consequence, they concluded that the GSSP-based definition of the Lutetian Stage would imply that part of the referential Lutetian deposits of the historical stratotype area should now be considered Ypresian in age, which they concluded to be a *contradictio in terminis*. In order to solve the supposed contradiction, they suggested re-defining the Lutetian GSSP using the LO of *Discoaster sublodoensis* as a marker event. Finally, the astronomical tuning of some pelagic records suggested that the C21r.6 position assigned to the current GSSP level should correspond to an older absolute age than that derived from Gorrondatxe (48.15 Ma according to Franceschi et al., 2015; 48.30 Ma according to Westerhold et al., 2017; 48.07 Ma in Speijer et al., 2020).

Consequently, in order to address the issues raised, we revisited the Gorrondatxe section. Taking into account the stratigraphic aspects that had been disputed, our study aimed to refine the magnetostratigraphy around the GSSP, clarify the stratigraphic range of key calcareous nannofossil species, and develop an astronomically tuned age model.

2. Geological setting and previous studies

The Gorrondatxe section is part of a 2300 m thick succession that accumulated at approximately 1500 m water depth and 35°N paleolatitude in Eocene times (Bernaola et al., 2006; Payros et al., 2006, 2007, 2009, 2011, 2012, 2015; Payros and Pujalte, 2020; Martínez-Braceras et al., 2021, 2023). The Ypresian–Lutetian transition interval extends from 900 to 1100 m (equivalent to 0 and 200 m, respectively, in this study) and contains the GSSP level at 967.85 m (herein 67.85 m; Fig. 1B). This succession is composed of hemipelagic marls and limestones with abundant intercalations of turbidites, generally just a few centimetres thick. Details on biomagnetostratigraphy, summarized in Fig. 1, can be found in Bernaola et al. (2006), Payros et al., (2006, 2007, 2009) and Molina et al. (2011). Most significantly for this study, the LOs of *Blackites piriformis*, *B. inflatus* and *Nannotetrina cristata* were found at 53.00, 67.85 and 78.00 m, respectively, the highest continuous occurrence of *Discoaster lodoensis* at 134.50 m, and the C21r/C21n chron reversal at an inconclusive interval with mixed polarities between 120.00 and 150.00 m. The stratigraphic distribution of turbidites is not uniform and, consequently, the sedimentary thickness between successive biomagnetostratigraphic events does not reflect directly the time elapsed. In order to obtain a time-related succession of events, Payros et al. (2007) aimed to remove the thickness represented by turbidites, assuming that the sedimentation rate of the remaining hemipelagic-only hypothetical succession would have been more constant. To this end, given the difficulty of measuring all centimetre thick turbidites, they compromised and calculated the turbiditic percentage in a 1 m thick interval of each 10 m thick slice of the section and extrapolated that percentage to the rest of the 10 m thick stratigraphic slice.

Payros et al. (2007, 2009) observed that the succession is organized in alternating intervals dominated by marly and limy hemipelagic deposits, which allowed the definition of marl-limestone couplets (Fig. 1B; supplementary Fig. S1). In the first 45.10 m of the Ypresian−Lutetian succession, they defined 22 couplets, each 1.10–3.10 m thick (average: 2.10 m), and a further 20 couplets in the 51.80–120.00 m interval, each 1.90–5.60 m thick (average: 3.20 m). The intervening section between 45.10 and 51.80 m is overgrown but Payros et al. (2009), on the basis of average couplet thickness, estimated it to contain three further couplets. They also noticed that the hardness of the marl-limestone couplets (a proxy for their carbonate content; see Payros and Martínez-Braceras, 2014, and Martínez-Braceras et al., 2017) varies cyclically, defining ten bundles of four to six couplets (Fig. 1B). The thickness of the five bundles in the lower part of the succession (0–45.10 m) varies between 9.00 and 10.20 m (average: 9.90 m), while the five bundles in the upper part (51.80–120.00 m) are thicker (10.70–14.70 m; average: 13.40 m). Using the age model derived from the available biomagnetostratigraphy, the marl-limestone couplets were considered to be the expression of ~20-ky-long precession cycles (the combination of 24–21 and 19–18 ky-long components) and the bundles the expression of ~100-ky-long short-eccentricity cycles (the combination of 125 and 95 ky-long terms). The wide range of couplet and bundle thickness was attributed to the variable distribution of intercalated turbidites, which was also astronomically forced (Payros and Martínez-Braceras, 2014; Martínez-Braceras et al., 2017). The supra-regional significance of the Gorrondatxe hemipelagic cycles was demonstrated by their correlation with coeval cycles from other sedimentary basins (Payros et al., 2011, 2012).

3. Materials and methods

3.1. Calcareous nannofossil biostratigraphy

The calcareous nannofossil biostratigraphic data is based on the analysis of 60 samples. All the samples were prepared as smear slides following standard methods (Bown & Young, 1998) and analyzed using a Zeiss Axioplan transmitted-light microscopy at 1600 magnification. Additionally, the smear-slides were also examined at 2000 magnification in order to detect smaller species, observe greater detail, and for photographic purposes. The standard schemes of Okada and Bukry (1980) and Agnini et al. (2014) and the standard taxonomy for Cenozoic calcareous nannofossils (Perch-Nielsen, 1985; Young & Bown 1997; Bown, 2005; Agnini et al., 2014) have been followed for this study. Further details can be found in supplementary Tables S1, S2, S3 and S4.

Twenty of the samples (from Az-825 to Az-1111) had previously

been analyzed by Bernaola et al. (2006) and have been re-studied herein in order to determine the position of calcareous nannofossil bioevents that were not reported in the original work but are now known to occur at the Ypresian/Lutetian transition (Supplementary Table S2). Firstly, a quantitative study was carried out in which a minimum of 300 autochthonous specimens were counted per sample. In a second round, five tracks (14.7 mm^2) per sample were analyzed in order to detect rare species and to determine changes in the abundance of taxa with key biostratigraphic value. Only the species in which changes in abundance have biostratigraphic significance were counted. Once the counting was completed, the number of specimens per mm^2 was calculated and rounded up following standard practice (Table S2).

Forty new samples were collected between 43 and 87 m with the aim of recording the bioevents that are closest to the Lutetian GSSP more accurately (i.e. the LOs of *B. piriformis*, *B. inflatus*, *N. cristata* and *D. wemmelensis*, the highest occurrence of *B. piriformis*, and the highest common occurrence of *G. gammation*). Five tracks were also studied in these samples, but generally only the presence or absence of the taxa under study was determined. The only exception is *G. gammation,* for which a specific count was carried out to determine its highest common occurrence. As in the original 20 samples, the result of this count is expressed as specimens per mm^2 and rounded up (Table S3).

Four types of biohorizons were defined. The lowest occurrence (LO) and the highest occurrence (HO) refer to the lowest and highest continuous occurrences of taxa, respectively. It was considered that the occurrence of a taxon is continuous when it appears in a series of successive samples, even if it may be absent in a few interspersed levels. The lowest common occurrence (LCO) and the highest common occurrence (HCO) of a species mark the levels where its abundance crosses the threshold of 6–9 specimens per mm^2 and changes significantly (an increases of 150% and a decrease of −75%, respectively). The LO, LCO, HCO and LO positions were defined at the mid point between two successive samples, the possible margin of error being expressed by the stratigraphic distance to the closest underlying and overlying samples (Supplementary Table S4).

3.2. Magnetostratigraphy

Data from the 45 samples originally analyzed for the magnetostratigraphic study of the Ypresian/Lutetian boundary interval were appraised in this work. In order to improve existing resolution, 21 new stratigraphic levels were sampled for further paleomagnetic analysis (Supplementary Table S5). The new sampling focused on hemipelagic lithologies, from which hand samples were collected and oriented in situ with a magnetic compass. For the paleomagnetic analysis, 29 standard cubic specimens were prepared in the laboratory from the 21 samples. Natural remanent magnetization (NRM) and remanence through demagnetization were measured using a 2G Enterprises DC SQUID high-resolution pass-through cryogenic magnetometer (manufacturer noise level of 10^{-12} Am^2) operated in a shielded room at the Istituto Nazionale di Geofisica e Vulcanologia in Rome, Italy. A pyrox oven in the shielded room was used for thermal demagnetization and alternating field (AF) demagnetization was carried out with three orthogonal coils installed in line with the cryogenic magnetometer. After a single heating step to 150 °C, progressive AF demagnetization was carried out in 14 steps (at 1, 8, 13, 17, 21, 25, 30, 35, 40, 45, 50, 60, 80, 100 mT). Characteristic remanent magnetizations (ChRM) were computed by least squares fitting (Kirschvink, 1980) on the orthogonal demagnetization plots (Zijderveld, 1967). The ChRM declination and inclination were used to derive the latitude of the virtual geomagnetic pole (VGP) of each sample considering their actual location. VGP latitudes express the original magnetic polarity of samples, as positive VGP latitudes represent normal polarity and negative VGP latitudes indicate reverse polarity (Table S6).

3.3. Cyclostratigraphy

With the aim of carrying out a cyclostratigraphic analysis of the first 120.00 m of the Ypresian/Lutetian boundary interval, 266 hand samples of 25–50 g were collected (Supplementary Table S7). To counter the samples not being evenly distributed throughout the succession, a minimum of three samples were collected from each hemipelagic marly and limy interval (i.e., minimum of six samples per marl-limestone couplet), avoiding interbedded turbiditic deposits. The samples were analyzed for bulk low-field magnetic susceptibility measurements using a Kappabridge MFK-1 (Agico) instrument housed at the University of the Basque Country, the results subsequently being weight-normalized and expressed as mass susceptibility (m^3/kg). The magnetic susceptibility of hemipelagic deposits is commonly determined by paramagnetic phases (mostly detrital clays) and generally anticorrelates with carbonate content, thus allowing spectral analysis of alternating successions for cyclostratigraphy (Kodama and Hinnov, 2015). To this end, the thickness represented by turbidites should ideally be subtracted from the succession (e.g. Weedon, 2003). It was not possible to measure all the turbidites in the Gorrondatxe section due to their abundance and thin-bedded nature (e.g., the 21 m thick interval studied in detail by Payros and Martínez-Braceras, 2014, contains 179 turbidites, each 0.1–5 cm thick). As an alternative, the turbidite percentages estimated by Payros et al. (2007) for each 10 m thick stratigraphic slice were subtracted, the actual 120 m thick succession thus becoming reduced to a hypothetical hemipelagic-only succession 36.60 m thick (Table S7). Subsequently, two independent cyclostratigraphic analyses were undertaken, one for the actual succession (including turbidites, assuming that their regular, astronomically forced distribution in the section does not produce a significant distortion in the thickness of cycles) and the other for the hypothetical hemipelagic-only section.

The cyclostratigraphic analysis was carried out using Acycle software (Li et al., 2019; available at https://acycle.org/) and the Astrochron package for R (Meyers, 2014). As samples were not evenly distributed along the succession, both the actual and the hemipelagic-only magnetic susceptibility records were linearly interpolated and detrended. Power spectrum analysis of the two detrended data series was carried out following the 2π-Multi Taper Method (MTM) with three tapers, and confidence levels were calculated using robust red-noise modelling (Mann and Lees, 1996; Meyers, 2012; Thomson, 1982). Given that the variations in couplet and bundle thickness suggest potential changes in sedimentation rate between the lower (0–42.70 m) and upper (51.70–119.10 m) parts of the succession, additional power spectrum analyses were carried out for each interval. Furthermore, with the aim of identifying distinctive frequency and amplitude modulations, the data series from both the actual and hemipelagic-only successions were used for Evolutive Harmonic Analysis (EHA, which follows MatLab's Fast Fourier transform method; Thomson, 1982). For the identification of potential low frequency cycles, Morlet wavelet analysis of the entire succession was performed (Torrence and Compo, 1998), as periods are represented in logarithmic scale. Subsequently, in order to determine the most likely sedimentation rates, the correlation coefficients (COCO) between the power spectra of astronomical solutions and the magnetic susceptibility data series were estimated separately for the lower and upper parts of the actual and hemipelagic-only successions. Finally, Gaussian bandpass filtering of the data series was undertaken in order to isolate the signal of the most significant frequencies. In order to tune the Gorrondatxe results astronomically, minima in the Gorrondatxe short-eccentricity filter outputs were prospectively correlated with minima from different intervals of the ZB18a orbital solution (Zeebe and Lourens, 2019). The root-mean-square deviation (RMSD) of each potential tuning was calculated with the aim of determining their accuracy and reliability (Zeebe and Lourens, 2019).

4. Results

4.1. Calcareous nannofossil biostratigraphy

Calcareous nannofossils from the Gorrondatxe section are in general well preserved. In some cases even delicate structures and coccospheres were found to be present (Fig. 2). As noted in previous studies (Bernaola et al., 2006; Molina et al., 2011; Intxauspe-Zubiaurre et al., 2017a, 2017b), assemblages are rich and diverse (including some allochthonous and reworked specimens), with an average of 45 species per sample and 17 specimens per field of view. Based on the autochthonous components of the assemblages (Fig. 3), the studied succession is assigned to zones

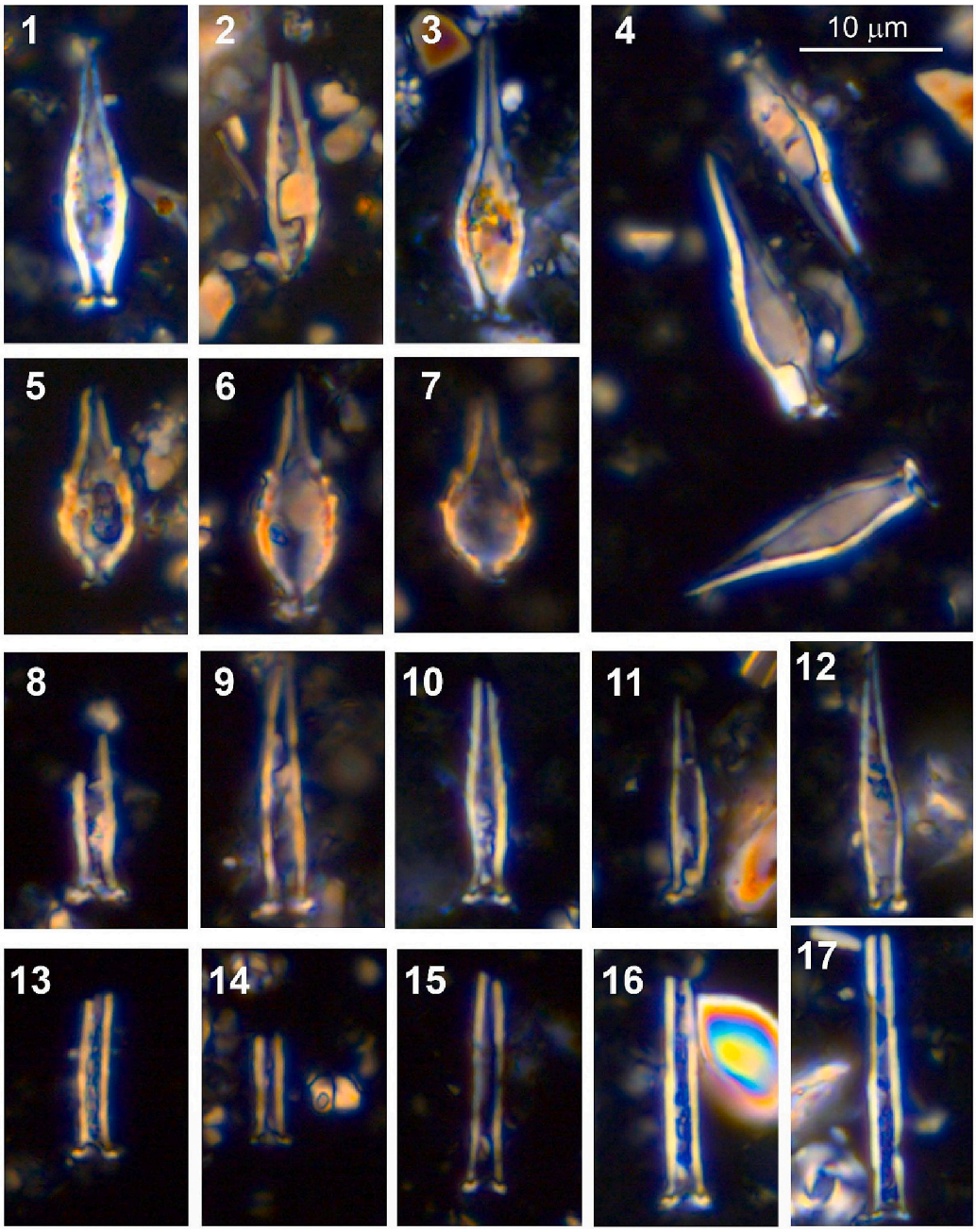

Fig. 2. Selected calcareous nannofossils from Gorrondatxe. The scale bars represent 10 μm in all figures. XPL: cross-polarized light; PL: plane polarized light. (A) 1–4: *Blackites inflatus* (1: Az-1102, 102.00 m, XPL; 2: Go-d, 67.85 m, XPL; 3: Az-987, 87.00 m, XPL; 4: Az-1115, 115.00 m, XPL). 5–7: *Blackites piriformis* (5: Go-5, 53.40 m, XPL; 6: Az-696, 69.00 m, XPL; 7: Az-961, 61.00 m, XPL). 8–12: *Blackites praeinflatus* (8: Az-860, −40.00 m, XPL; 9: Az-943, 43.00 m, XPL; 10 & 11: Az-1102, 102.00 m, XPL; 12: Az-1115, 115.00 m, XPL). 13–17: *Blackites tenuis* (13: Az-850, −50.00 m, XPL; 14: Az-961, 61.00 m, XPL; 15: Az-987, 87.00 m, XPL; 16 & 17: Az-1102, 102.00 m, XPL). (B) 1–5: *Blackites spinosus* (1 & 2: Az-943, 43 m, XPL; 3: Az-969, 69.00 m, XPL; 4: Az-987, 87.00 m, XPL; 5: Az-1002, 102.00 m, XPL). 6: *Discoaster lodoensis* (Az-890, −10.00 m, PL). 7–8: *Blackites inversus* (7 & 8: Az-987, 87.00 m, XPL; 8: rotated 45°). 9–10, 14–15: *Discoaster sublodoensis* (9: Az-918, 18.00 m, PL; 10: Az-860, −40.00 m, PL; 14: Az-961, 61.00 m, PL; 15: Az-890, −10.00 m, PL). 11–13, 16–18: *Discoaster wemmelensis* (11: Az-969, 69.00 m, XPL; 12: Az-969, 69.00 m, PL; 13: Az-987, 87.00 m, XPL; 16: Az-1115, 115.00 m, XPL; 17: Az-1115, 115.00 m, PL; 18: Az-987, 87.00 m, PL). 19–23: *Discoaster kuepperi* (all from Az-825, −75.00 m; 19 & 21: XPL; 20 & 22: PL; 23: XPL, lateral view). (C) 1–9: *Girgisia gammation* (1: Az-961, 61.00 m, XPL; 2: Az-961, 61.00 m, PL; 3: Az-825, −75.00 m, XPL; 4: Az-825, −75.00, PL; 5: Az-943, 43.00 m, XPL.; 6: Az-918, 18.00 m, XPL; 7: Az-918, 18.00 m, PL; 8: Az-943, 43.00 m, XPL; 9: Az.943, 43.00 m, PL). 10–13: *Nannotetrina cristata* (10: Go-cris-5, 74.00 m, PL; 11: Az-1113, 113.00, PL; 12: Go-cris-6, 75.00 m, PL). 14–15: *Nannotetrina fulgens* (Az-1246, 346.00 m, PL). 16–19: *Chiasmolithus gigas* (all from Az-1319, 419.00 m; 16 & 17: XPL; 18 & 19: PL).

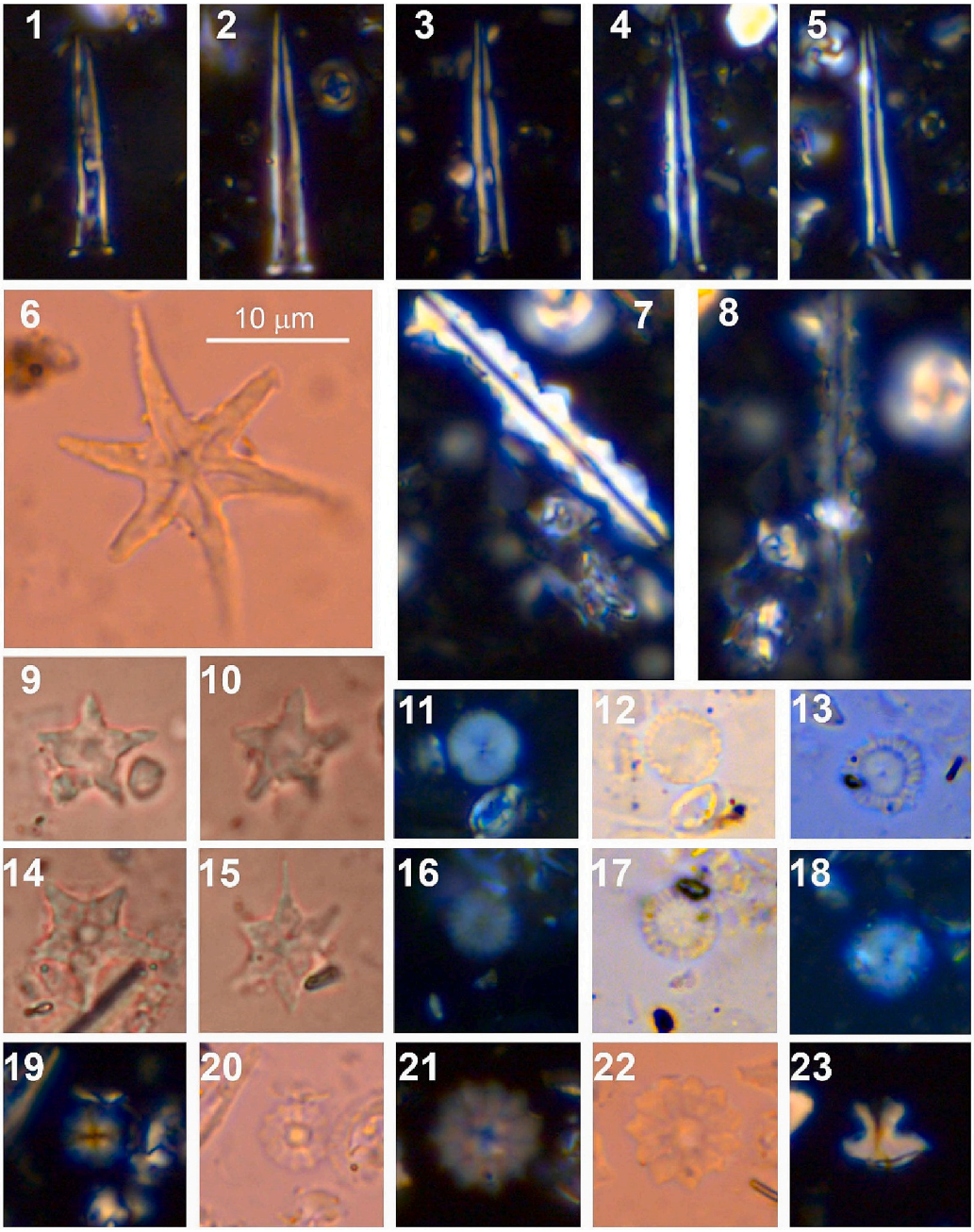

Fig. 2. (*continued*).

CNE6-CNE8 of Agnini et al. (2014) and subzones CP12a and CP12b of Okada and Bukry (1980). In fact, Bernaola et al. (2006) found the LO of five-rayed *Discoaster sublodoensis* (base of CP12a) to be located at 832.50 (±7.50) m of their succession (i.e., −67.50 ± 7.50 m below the interval studied herein) and that of *Blackites inversus* at 870.00 (±10.00) m (i.e., at −30.00 ± 10.00 m in this study).

In the studied interval, the HCO of *Discoaster lodoensis* was found at 25.50 (±7.50) m (see supplementary Table S4 for further details on biostratigraphic events). After a sharp decline in abundance at this level, *D. lodoensis* is continuously present (1–3 specimens per sample) up to 134.50 m. Following Cappelli et al. (2019), the HCO of *D. lodoensis* was used to mark the base of Zone CNE7, rather than its HO (Agnini et al., 2014). The LO of *Blackites praeinflatus* was defined at 38.00 (±5.00) m (Fig. 3). The LO of *Blackites piriformis* was located at 53.20 (±0.20) m, and that of *Discoaster wemmelensis* at 55.90 (±0.30) m. The LO of *Blackites inflatus*, the marker event of the base of Subzone CP12b and the Lutetian GSSP level, was confirmed to be at 67.85 (±0.10) m, as stated in previous studies (Molina et al., 2011). The HCO of *Girgisia gammation* was found at 70.50 (±0.50) m and its HO at 108.50 (±6.50) m. The HO of *B. piriformis* was found at 71.50 (±0.50) m. The LO of *Nannotetrina cristata*, the marker event of the base of Zone CNE8, was identified at 73.50 (±0.50) m. The HO of *Discoaster kuepperi* was determined to be at 159.50 (±5.50) m. Finally, the HCO of *B. inflatus* was established at 172.00 (±7.00) m.

The stratigraphic positions previously provided for other zonal markers (LO of *Nannotetrina alata* group as base of Subzone CP13a and Zone CNE9, and LO of *Chiasmolithus gigas* as base of Subzone CP13b and Zone CNE10; Bernaola. et al., 2006, and Molina et al., 2011) are also confirmed in this study (Fig. 3). In order to assess the chronostratigraphic reliability of the results, the sequence of calcareous nannofossil events identified in Gorrondatxe was compared with that found in other sections (Fig. 3).

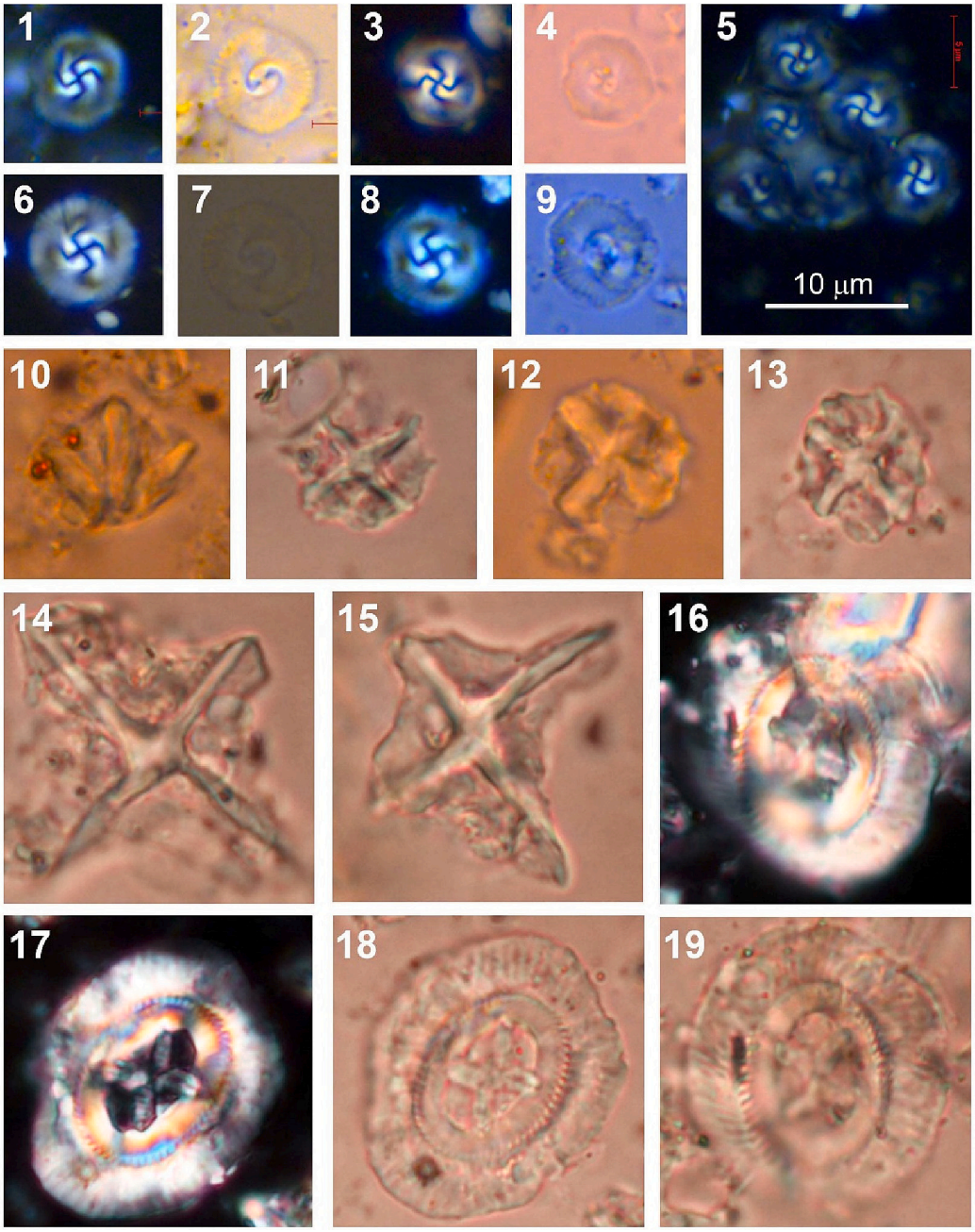

Fig. 2. (*continued*).

4.2. Magnetostratigraphy

The NRM intensity of the Gorrondatxe samples ranges from 0.02 to 0.1 mA/m, showing no significant variations along the section. During demagnetization, the NRM intensity of the samples decreased significantly after the first heating step at 150 °C and proceeded up to around 4–17 mT, demagnetizing a component which is usually northerly oriented and steep in in-situ (geographic) coordinates (Fig. 4A). Given that this low-field component conforms to a recent viscous geomagnetic field direction in geographic coordinates, it is regarded as secondary overprinting. Above this low field, demagnetization trajectories trended toward the origin up to about 80–100 mT. These demagnetization trajectories were used to define the ChRM components, which were either northerly and moderately steeply downward oriented, or southerly and upward oriented in bedding corrected coordinates. As the Gorrondatxe strata are subvertical, it is reasonable to conclude that these ChRM components originated before tectonic tilting and therefore represent a primary magnetization with dual polarity. In fact, these ChRM directions have no geological significance in in-situ (geographic) coordinates.

Demagnetization data from 33% of the Gorrondatxe samples (25 out of 75 specimens; Fig. 4B and Supplementary Table S6) showed low magnetic intensity or random trajectories upon demagnetization, and were consequently classified as 'class C' (indicated by crosses in Fig. 4B). 'Class B' samples (open circles in Fig. 4B) are those in which a magnetic component could be calculated but the result was regarded as unreliable either because demagnetization trajectories were not sufficiently straight and/or did not trend toward the origin of the demagnetization diagram (21 specimens, 28%; Supplementary Table S6). The rest of the samples (29 specimens, 39%; Supplementary Table S6) provided reliable ChRM components suitable for magnetostratigraphy, therefore being referred to as 'class A' (closed circles in Fig. 4B). The results from

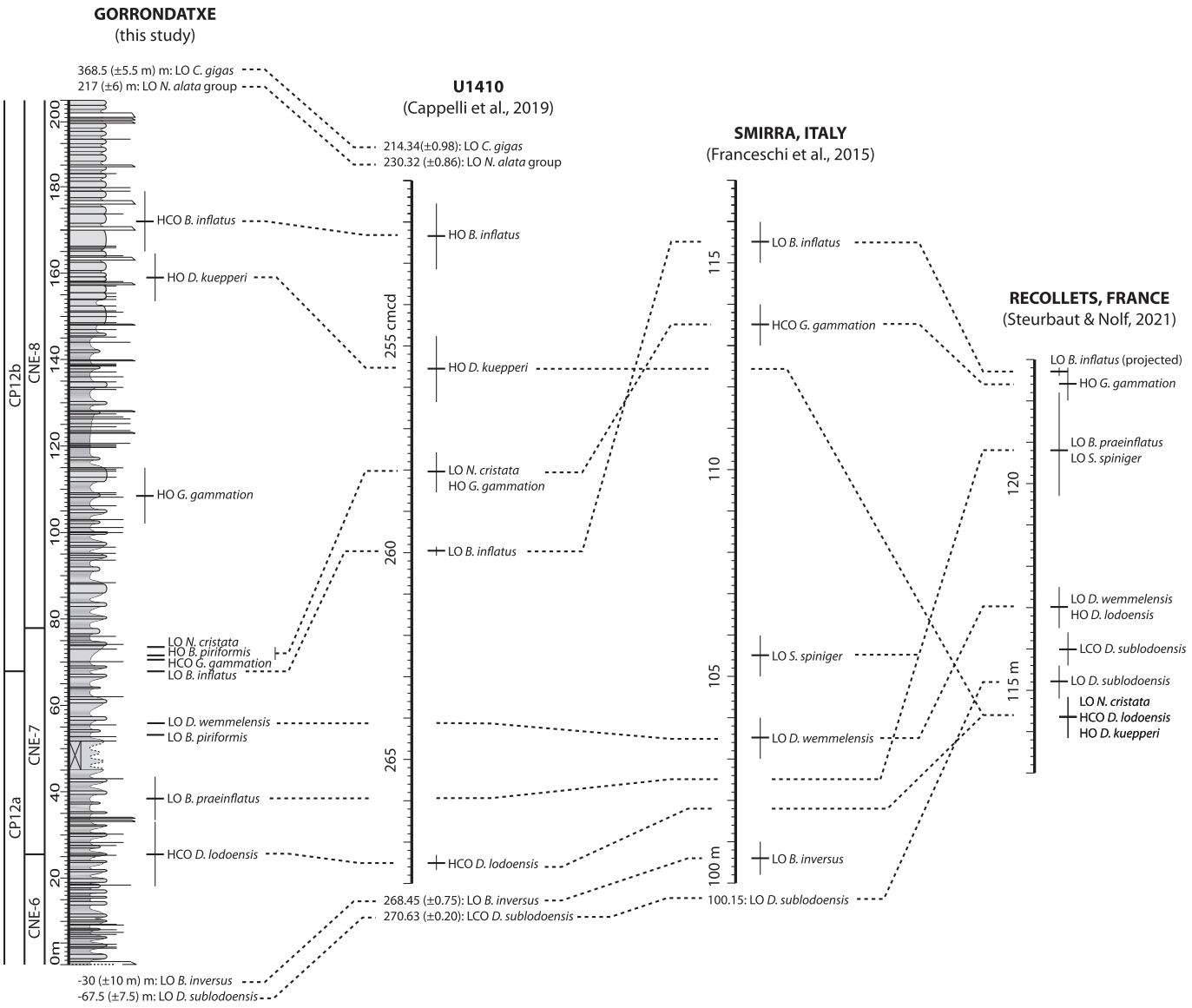

Fig. 3. Stratigraphic distribution of the most significant calcareous nannofossil events of the Gorrondatxe section and correlation with other reference sections.

'class A' samples indicate that the 0–120.00 m interval of the Gorrondatxe section is consistently of reverse polarity (Fig. 4; Supplementary Table S6). This interval is attributed to Chron C21r on the basis of the biostratigraphic results. From 135.00 m upwards, another interval characterized by consistent normal polarity is attributed to Chron C21n. Samples from three levels of the intervening interval (121.00, 123.00 and 124.00 m) yielded normal polarity, but one sample (two specimens analyzed) from a higher level (134.00 m) showed reverse polarity (Fig. 4B; Supplementary Table S6).

As they are, these findings do not help pinpoint the C21r/C21n reversal boundary. The actual C21r/C21n chron boundary could be located at 120.50 m if the reverse result from 134.00 m were an artefact. However, it should also be taken into account that during a magnetostratigraphic transition from an older reverse to a younger normal chron, delayed magnetization acquisition can occur given the post-depositional remanent magnetization lock-in process (e.g. Roberts and Winklhofer, 2004). In such a scenario, samples which show a normal magnetic polarity and are succeeded upsection by others showing reverse polarity, strongly suggest delayed magnetization acquisition during the time of a younger normal chron (e.g., Dinarès-Turell and Dekkers, 1999; Payros et al., 2011; Suganuma et al., 2010; and references therein). In the case of Gorrondatxe, given that there is just one level with reverse polarity at 134.00 m, we consider the magnetic polarity of the 120.50–134.50 m interval to be inconclusive, the actual C21r/C21n reversal boundary possibly being located anywhere between its bottom and its top.

4.3. Cyclostratigraphy

Weight-normalized magnetic susceptibility values range from 1.87 $\times$ 10^{-6} m^3/kg to 7.46 $\times$ 10^{-6} m^3/kg (average: 4.54 $\times$ 10^{-6} m^3/kg), lower values generally corresponding to limestone samples and higher values corresponding to marl samples (Fig. 5A; Supplementary Table S7). This suggests that magnetic susceptibility is mostly determined by paramagnetic phases (detrital clay minerals), the data series thus being suitable for cyclostratigraphic analysis.

The 2π-MTM power spectrum of the linearly interpolated and detrended (3rd order polynomial fit) actual data series (including turbidites) shows significant peaks above 99% confidence level (CL) at three frequency intervals: 1.80 m, 2.80 m and 12.00 m (Fig. 5B). The power spectrum from the lower part of the succession (0–42.70 m) shows a prominent peak (>99% CL) at 2.3 m and another less prominent

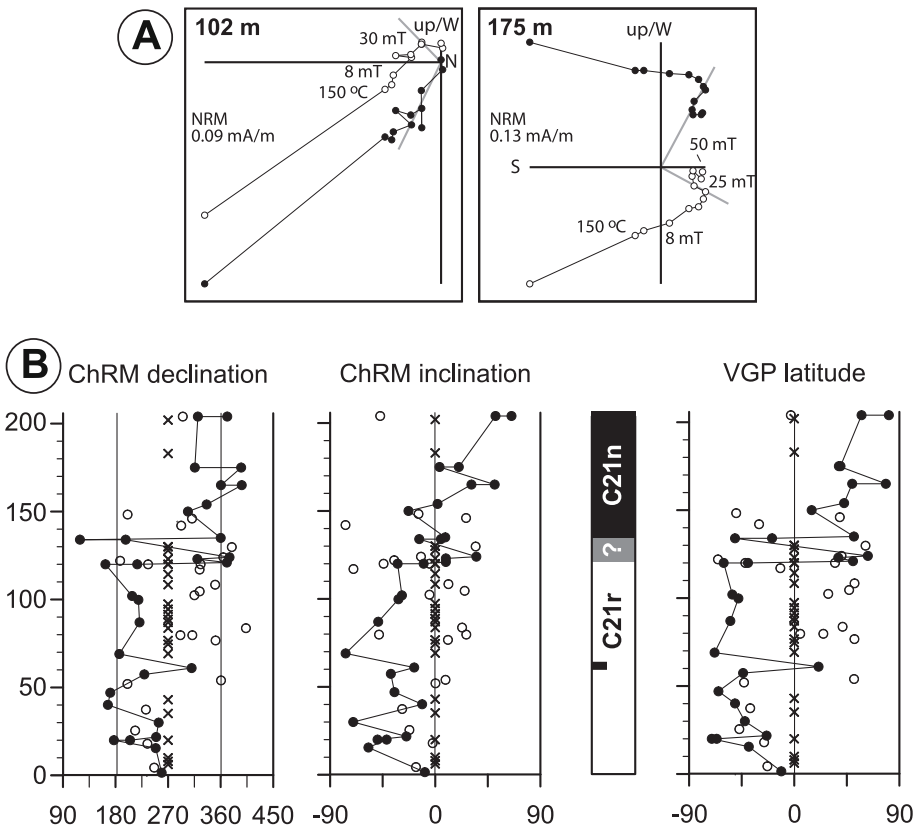

Fig. 4. (A) Examples of tilt-corrected orthogonal demagnetization diagrams of two class A samples of the Gorrondatxe section, representative of reverse and normal magnetic polarity (stratigraphic layers at 102.00 and 175.00 m, respectively). The natural remanent magnetization (NRM) intensity and relevant demagnetization steps are indicated. Open and closed circles indicate projections onto the upper and lower hemispheres, respectively. The computed characteristic remanent magnetization (ChRM) direction is shown by a thick grey line. (B) Declination and inclination plots of the ChRM components. Crosses indicate class C specimens (no data), open circles denote class B specimens (unreliable directions), and closed circles mark class A specimens (reliable directions). The virtual geomagnetic pole (VGP) latitude defines the magnetostratigraphy, which includes a lower reverse polarity zone (0–120.50 m, correlated with Chron C21r) and an upper normal polarity zone (134.50–200.00 m, correlated with Chron C21n). In the intervening inconclusive interval, three stratigraphic levels (121.00, 123.00 and 124.00 m) yielded normal polarity while another level (134.00 m) showed reverse polarity.

peak, but still above 90% CL and almost reaching 95%, at 10.10 m. The power spectrum from the upper part of the succession (51.70–119.10 m) shows a prominent double peak (>99% CL) at 2.80 and 3.50 m (average: 3.20 m) and another less prominent peak (above 90% CL, approaching 95%) at 16.00 m. These periodicities match the average thicknesses measured in each part of the succession for the limestone-marl couplets attributed to precession cycles and the bundles attributed to short eccentricity cycles. Accordingly, the periodicities match the 1:5 ratio that characterizes successions forced by short eccentricity (~100 ky) and precession (~20 ky) cycles. The fact that the bundle-related peaks are not as prominent as the couplet-related peaks in the 2π-MTM power spectra of the lower and upper parts of the section can be attributed to both intervals being relatively short.

The wavelet spectrum of the entire succession confirms the occurrence of metre-scale cycles related to precession couplets, the period of which shifts from approximately 2.00 m in the lower part of the succession to 3.00 m in the upper part, and a bundle-related band at the 13.00–14.00 m period (Fig. 6A). The power of the bundle-related band in the wavelet spectrum is discontinuous, showing reduced power around the covered part of the succession and at the top of the succession. Despite being out of the cone of influence in the area where edge effects become important, another high-power band occurs at the 50.00 m period.

Although the bundle-related peaks are generally not prominent in the 2π-MTM power spectra, the frequency bands related to the eccentricity bundles are the most prominent in all evolutionary EHA spectra (Fig. 6). Interestingly, these bands also show disruptions at specific intervals (namely, at approximately 12.00–20.00 m, 60.00–70.00 m, and above 90.00 m), represented as either decreases in power or band bifurcations. The frequency band related to precession couplets is also well represented in all EHA spectra. Furthermore, some discontinuous intermediate bands also occur in the evolutionary spectra at the 3.70 m period in the lower part of the succession and at the 4.50–5.60 m period in the upper part of the succession.

In order to determine the most likely sedimentation rates and to estimate the duration of the cycles identified in the spectral analyses, the correlation coefficients (COCO) between the power spectra of the Gorrondatxe magnetic susceptibility data series and astronomical solutions were estimated separately for the lower and upper parts of the section (Fig. 7). In each case, 5000 Monte Carlo simulations were run, 712 sedimentation rates being tested between 3.9 and 75.0 cm/ky with 0.1 cm/ky steps. The optimal sedimentation rate in the lower part of the succession is 10.9 cm/ky (Fig. 7A). Accordingly, the 2.30 m cycles identified in the 2π-MTM and EHA spectra would represent ~21 ky, the 10.10 m bundles representing ~93 ky (Table 1). The 3.70-m-thick cycles identified in the EHA spectrum of the lower part of the succession represent 34 ky. The optimal sedimentation rate in the upper part of the succession is 13.3 cm/ky (Fig. 7B). This sedimentation rate implies that the 3.20-m-thick couplets from the upper part of the succession represent ~24 ky (Table 1). The 16.00-m-thick periodicity identified in the 2π-MTM spectrum represent ~120 ky; however, if the 13.50 m bundle period defined visually in the upper part of the succession and in the wavelet spectrum were taken into account, bundles would represent ~101 ky. In addition, the approximately 5.00-m-thick cycles identified in the EHA spectrum of the upper part of the succession represent ~38 ky. Finally, the 50.00-m-thick periodicity identified in the wavelet spectrum of the entire succession represents 413 ky if the average sedimentation rate of the lower and upper parts of the succession (i.e., 12.1 cm/ky) is considered (Table 1).

Similar analyses were carried out for the hypothetical pelagic-only succession (turbidites removed; see supplementary material). The 2π-MTM power spectra (supplementary Fig. S2), first performed for the entire succession and then for its lower and upper parts separately, show significant peaks (>95–99% CL) of 3.50–4.00 m and 0.65–0.80 m periods. These periodicities, which match a 1:5 ratio, correspond to the short eccentricity (~100 ky) bundles and precession (~20 ky) couplets in the hypothetical pelagic-only succession (Payros and Martínez-Braceras, 2014; Martínez-Braceras et al., 2017). Other less prominent peaks

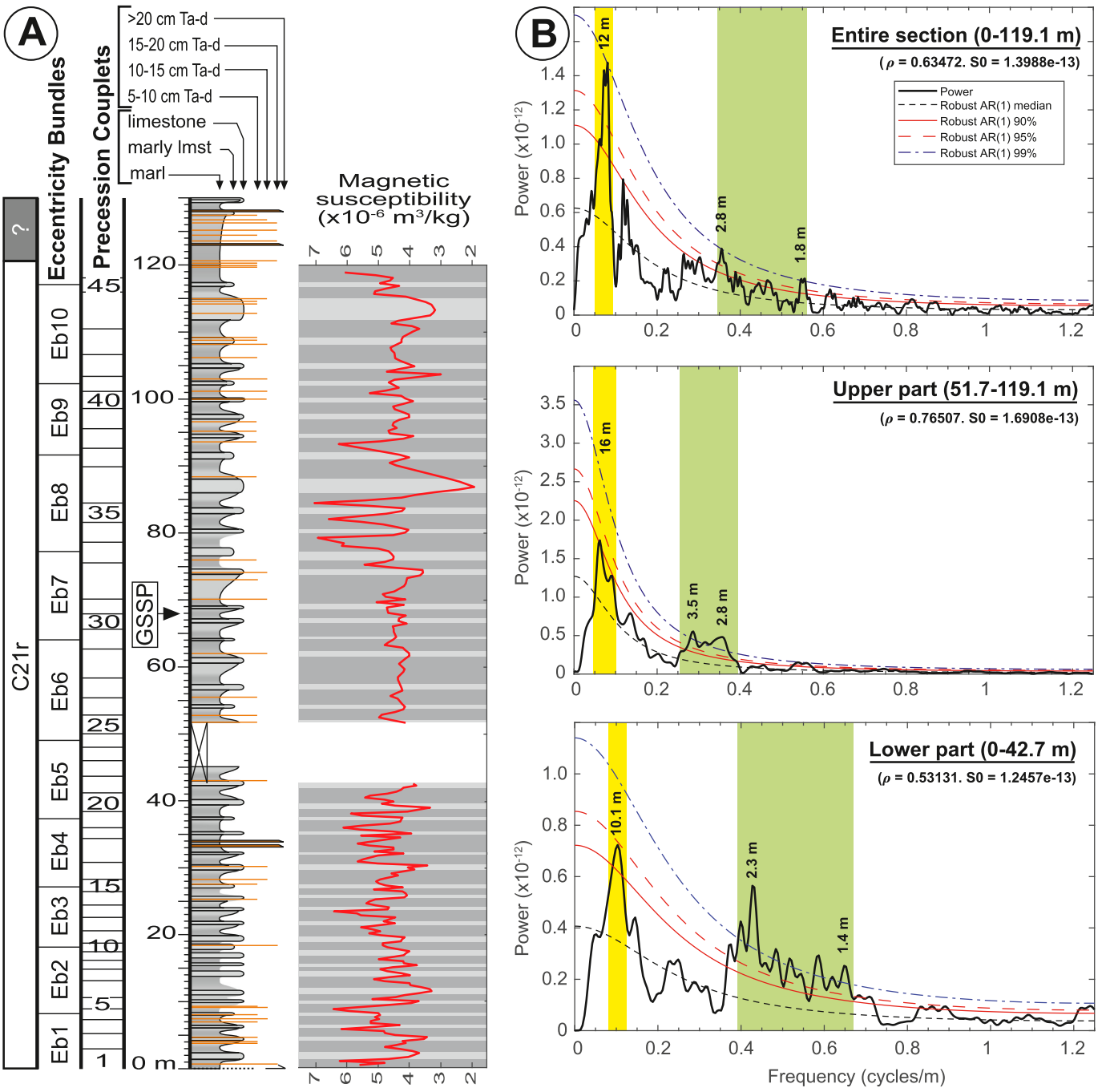

Fig. 5. (A) Stratigraphic log of the Ypresian/Lutetian interval analyzed for cyclostratigraphy in Gorrondatxe, with indication of magnetostratigraphy, eccentricity bundles (Eb) and precession couplets (Pc) defined visually by Payros et al. (2009), the GSSP level at the LO of *Blackites inflatus*, and the bulk low-field mass magnetic susceptibility obtained from hemipelagic bulk rock samples. This parameter varies in line with the lithological alternation, showing that it is determined by the abundance of detrital clay minerals and is suitable for cyclostratigraphic analysis. (B) 2π-MTM power spectra (black curves) of the bulk low-field magnetic susceptibility data series (interpolated linearly and detrended using a 3rd-order polynomial fit) showing median, 90%, 95% and 99% confidence levels for a red noise test (a fitted AR1 process). Top: entire succession (0–119.10 m); bottom: lower part of the succession (0–42.70 m); middle: upper part of the succession (51.70–119.10 m). The green and yellow areas include the most significant peaks (period values above), which can be related to the average thicknesses of precession (~20 ky) couplets and short (~100 ky) eccentricity bundles, respectively. (For interpretation of the references to colour in this figure legend, the reader is referred to the web version of this article.)

(90–95% CL), more clearly defined in the EHA spectra (supplementary Fig. S3), were found at 1.98 and 1.35 m periods. The wavelet spectrum of the entire pelagic-only succession successfully identifies the main periodicities mentioned above and, additionally, suggests the occurrence of a lower frequency band, with a period of 15.10 m, out of the cone of influence (supplementary Fig. S3A). The COCO analysis (2000 Monte Carlo simulations run, 329 sedimentation rates tested between 0.3 and 100 cm/ky with 0.3 cm/ky steps) yields an optimal sedimentation rate of 3.6 cm/ky (supplementary Fig. S4). Accordingly, the 3.50–4.00 m Gorrondatxe bundles represent 97–111 ky, and the 0.65–0.80 m couplets represent 18–22 ky (Table 1). The 1.35 and 1.98 m periodicities identified in the EHA spectra correspond to 38 and 55 ky, respectively, and the 15.10 m periodicity of the wavelet spectrum represents 419-ky cycles.

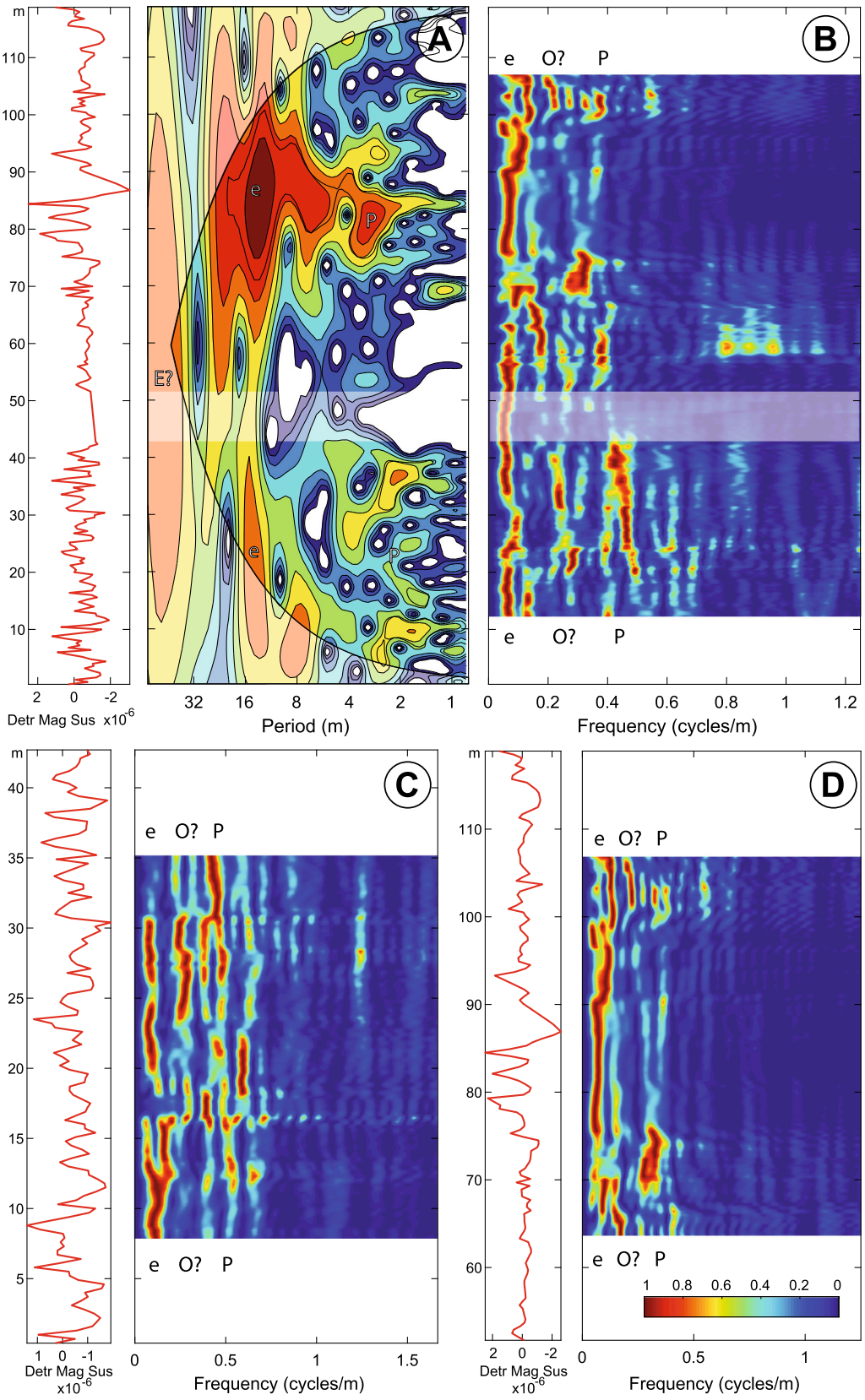

Fig. 6. (A) Wavelet power spectrum of the Gorrondatxe magnetic susceptibility data series. The cone of influence where edge effects become important is shown by the blurred area. (B) Evolutive harmonic analysis of the detrended magnetic susceptibility data series (sliding window of 23.68 m with steps of 0.40 m). Evolutionary spectra for the lower part of the succession (C: 0–42.70 m; sliding window of 15.00 m with steps of 0.30 m) and the upper part of the succession (D: 51.70–119.10 m, sliding window of 24.00 m with steps of 0.40 m) are also shown. The inferred Milankovitch components are represented by E (long eccentricity, ~405 ky), e (short eccentricity, ~100 ky), O (obliquity, ~38 ky) and P (precession, ~20 ky).

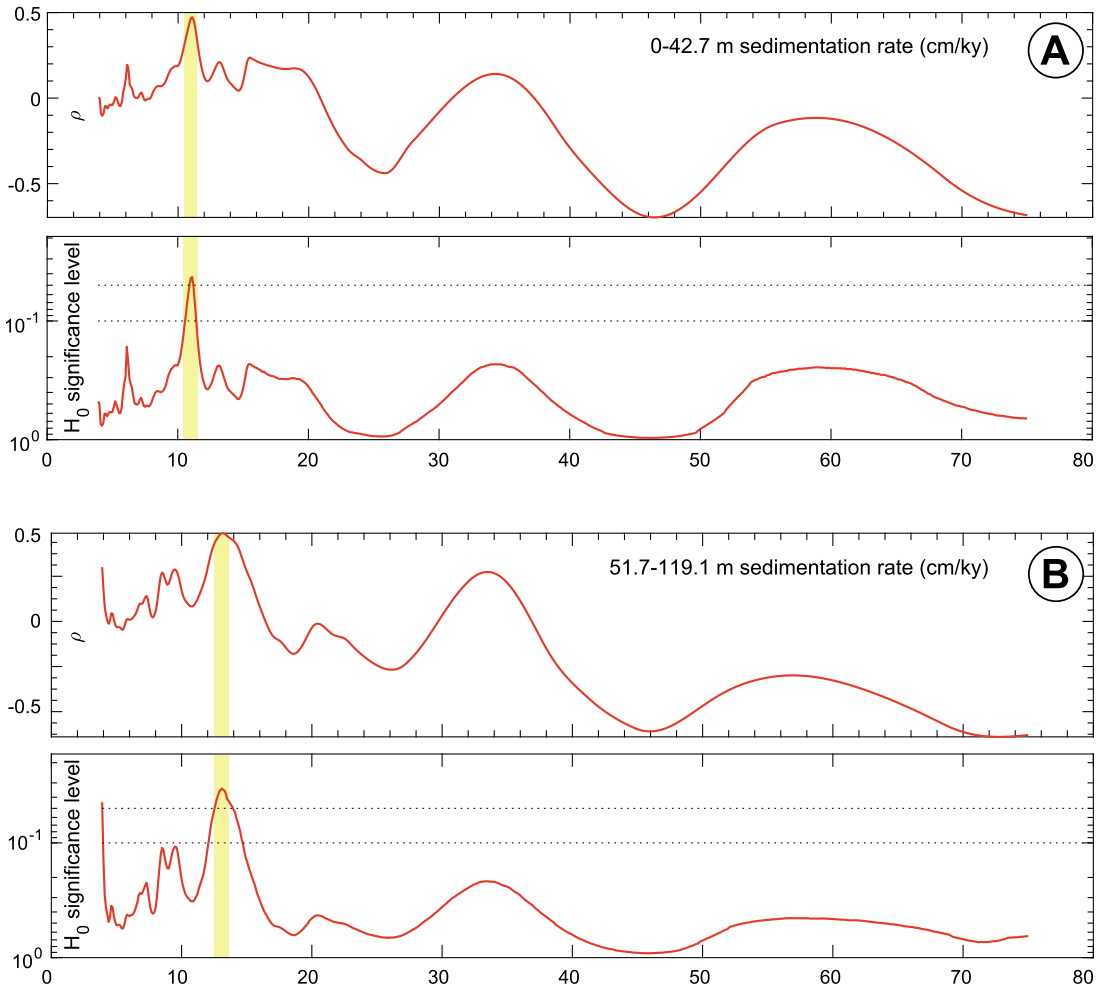

Fig. 7. Statistical estimation of sedimentation rates in the lower (0–42.70 m) and upper (51.70–119.10 m) parts of the Gorrondatxe section derived from the correlation coefficient (COCO) analysis between the power spectra of the analyzed data series and the Laskar et al. (2004) astronomical solution for 48 Ma. 5000 Monte Carlo simulations were run in each case, 712 sedimentation rates being tested between 3.9 and 75.0 cm/ky with 0.1 cm/ky steps, and the number of contributing astronomical parameters was seven (not shown). (A) Pearson correlation coefficient (ρ) and the null hypothesis (H_0) significance level of no astronomical forcing show that the optimal sedimentation rate is 10.9 cm/ky (yellow area) in the lower part of the Gorrondatxe section. (B) Pearson correlation coefficient (ρ) and the null hypothesis significance level (H_0) of no astronomical forcing show that the optimal sedimentation rate is 13.3 cm/ky (yellow area) in the upper part of the Gorrondatxe section. (For interpretation of the references to colour in this figure legend, the reader is referred to the web version of this article.)

5. Discussion

5.1. Astronomical forcing on sedimentation

In general, the intercalation of turbidites in hemipelagic successions hinders both cyclostratigraphic analysis and the identification of astronomical forcing on sedimentation. However, in Gorrondatxe Payros and Martínez-Braceras (2014) showed that the characteristics and stratigraphic distribution of turbidites were related to precession cycles (higher abundance, greater thickness and higher energy structures in turbidites interbedded in marly hemipelagic intervals due to increased terrestrial input during periods of increased seasonality, rainfall and runoff) and modulated by short-eccentricity cycles (higher contrast between turbidites from successive marl and limestone intervals at eccentricity maxima). The cyclostratigraphic analysis carried out herein confirms the astronomical forcing on the Gorrondatxe section and allows further elaboration of its chronostratigraphic framework.

The two main periodicities identified in the 2π-MTM, EHA and wavelet power spectra of both the actual and the hypothetical pelagic-only data series match the 1:5 ratio that characterizes successions forced by short eccentricity and precession cycles. This interpretation is further supported by the duration of the Gorrondatxe bundles and couplets, which was estimated on the basis of the average sedimentation rates calculated using COCO analysis (respectively ~100 and ~ 20 ky). In addition, the EHA spectra depict cycles of ~38 and ~ 55 ky, which could be related to forcing by obliquity. Finally, the wavelet spectra suggest the occurrence of cycles of 413–419 ky, most likely related to long (405 ky) eccentricity. This is supported by the amplitude modulation of the short (~100 ky) eccentricity frequency band in the EHA and wavelet spectra, as the disruptions (bifurcations and power reductions) observed at certain intervals (12.00–20.00 m, 60.00–70.00 m, and above 90.00 m) are common in long eccentricity minima nodes.

Taking the new evidence into account, it can safely be concluded that deep-marine sedimentation in the Gorrondatxe area was significantly influenced by precession and eccentricity cycles during Chron C21r. The influence of obliquity cycles was less significant in Gorrondatxe. This could be related to the relatively low latitude of the area in Eocene times, as obliquity is known to affect mainly high-latitude areas (Bosmans et al., 2015). Accordingly, most cyclostratigraphic analyses of Maastrichtian to early Ypresian successions of the area showed no evidence of obliquity forcing (Dinarès-Turell et al., 2002, 2003, 2007, 2010, 2012, 2014; Batenburg et al., 2012). Only in some cases, when the amplitude of eccentricity and precession cycles decreased at very long eccentricity minima, did the relative significance of obliquity increase

Table 1
Thickness and duration of the cycles identified by spectral analysis in the Gorrondatxe actual and pelagic-only sections.

Cycle type		Actual section		Pelagic-only section	
		Thickness	Duration	Thickness	Duration **
Long eccentricity cycles	Entire section	50 m	413 ky *	15.1 m	419 ky
Short eccentricity cycles	Entire section	12 m	99 ky *	3.5–4 m	97–111 ky
	Upper part	16 m, 13.5 m	120 ky, 101 ky ***	4 m	111 ky
	Lower part	10.1 m	93 ky ****	4.1 m	114 ky
Obliquity cycles	Entire section	3.7–5.6 m (av. 4.7 m)	av. 39 ky *	1.35 m, 1.98 m	38 ky, 55 ky
	Upper part	4.5–5.6 m (av. 5 m)	av. 38 ky ***	1.35 m, 2.0 m	38 ky, 56 ky
	Lower part	3.7 m	34 ky ****	1.31 m, 1.77 m	36 ky, 49 ky
Precession cycles	Entire section	1.8–2.8 m (av. 2.3 m)	av. 19 ky *	0.65–0.8 m	18–22 ky
	Upper part	2.8–3.5 m (av. 3.2 m)	av. 24 ky ***	0.63–0.86 m	18–24 ky
	Lower part	2.3 m	21 ky ****	0.67–0.72 m	19–20 ky

* Sedimentation rate: 12.1 cm/ky, average of the lower and upper parts, as derived from COCO.
** Optimal sedimentation rate (COCO) in the pelagic-only section: 3.6 cm/ky.
*** Optimal sedimentation rate (COCO) in the upper part: 13.3 cm/ky.
**** Optimal sedimentation rate (COCO) in the lower part: 10.9 cm/ky.

(Batenburg et al., 2014; Martínez-Braceras et al., 2023). However, similar to Gorrondatxe, the record of obliquity cycles has also been identified in other relatively low-latitude C21r successions (Westerhold and Röhl, 2009; Francescone et al., 2019). The occurrence of an obliquity signal in low-latitude Ypresian-Lutetian oceanic records could be related to the increasing influence of higher latitude processes in a progressively cooling Eocene Earth.

5.2. Astronomical tuning

Several different fully integrated astronomical solutions have been published to date (Laskar et al., 2004, 2011; Zeebe and Lourens, 2019). However, most of them show very similar short-eccentricity models for the 46–50 Ma interval that includes the Ypresian/Lutetian boundary (supplementary Fig. S5). In fact, the motion of the most significant astronomical bodies and their gravitational influence on the Earth's orbit throughout the last 50 Ma have been reliably solved. Consequently, a reliable astronomically calibrated time scale of the last 50 Ma is available, which allows the comparison and correlation (tuning) of local short-eccentricity records with astronomical solutions (Hinnov, 2013; Laskar, 2020; Laskar et al., 2011; Zeebe and Lourens, 2019).

The short-eccentricity component of the Gorrondatxe data series was extracted using Gaussian bandpass filtering. To this end, the frequency values identified in the 2π-MTM power spectra of both the actual and the pelagic-only data series were used, allowing sufficiently ample bandwidth. Similar filter outputs were obtained from both data series (Fig. 8 and supplementary Fig. S6). The filter outputs of the entire succession show eleven short eccentricity cycles (e1-e11), five from the lower part and the upper part of the succession (e1-e5 and e7-e11, respectively), plus another cycle (e6) in the intervening covered interval. Filter outputs obtained separately from the lower and upper parts of the section confirm this distribution. In addition, the long eccentricity components of both the lower and upper parts of the section were extracted (Fig. 8). The minima in the long eccentricity filter outputs (E1-E3) coincide with the covered part of the succession and with the intervals in which disruptions (bifurcations and power reductions) of the short-eccentricity frequency band occur in the EHA and wavelet spectra (see above). The sum of both the short and long eccentricity filter outputs was calculated in each interval (Fig. 8) and used for comparison with astronomical solutions.

To this end, the 46.9–49.9 Ma interval, which contains the C21r/C21n magnetic reversal and the Ypresian/Lutetian boundary (Speijer et al., 2020), was considered. Given that most short-eccentricity solutions for this interval are similar (supplementary Fig. S5; Laskar et al., 2011; Zeebe and Lourens, 2019), the comparison was restricted to the most recent solution ZB18a. Potential tuning to four different intervals of ZB18a was considered by correlating minima in the Gorrondatxe filter outputs and in the astronomical solution (Fig. 9; supplementary Table S8). In each case, the potential age of the LO of *B. inflatus* was obtained directly from the astronomical tuning. The C21r/C21n chron boundary cannot be astronomically tuned at Gorrondatxe. However, age estimates were obtained using the 13.3 cm/ky sedimentation rate obtained in the COCO analysis of the upper part of the Gorrondatxe succession.

Tuning option 1 (Fig. 9; supplementary Table S8) suggests that the LO of *B. inflatus* is located within the age range derived from other studies (Franceschi et al., 2015; Westerhold et al., 2017; Boulila et al., 2018; Speijer et al., 2020); however, the C21r/C21n magnetic reversal would be significantly younger, implying that the Gorrondatxe magnestostratigraphy is not reliable (as hinted in some previous studies; e.g. Westerhold et al., 2017; Cappelli et al., 2019). Based on tuning option 2, the ages of both the LO of *B. inflatus* and the C21r/C21n Chron boundary are close to the ranges derived from previous studies and almost identical to those in Speijer et al. (2020). Tuning option 3 places the C21r/C21n Chron boundary in a slightly older age than previous studies, although still within the estimated margin of error; however, the LO of *B. inflatus* is significantly older than in previous studies, suggesting that this bioevent is diachronus. Finally, tuning option 4 implies that both the LO of *B. inflatus* and the C21r/C21n Chron boundary are significantly older than previously estimated, rendering this an unlikely option.

The reliability of each potential tuning was determined by calculating the root-mean-square deviation (RMSD). Tuning options 1 and 2 yielded results that were deemed to be unreliable (RMSD >1 in Fig. 9; supplementary Table S8). Tuning option 4 yielded a lower RMSD value (0.980), however this option is highly unlikely due to the reasons mentioned above. The most favourable result was obtained from tuning option 3 (RMSD: 0.865). Accordingly, the Lutetian GSSP at the LO of *B. inflatus* (67.85 m) in Gorrondatxe can be tuned at 48.455 Ma, the base of the inconclusive magnetostratigraphic interval can be age dated at 48.073 (±0.004) Ma, and the top at 47.968 (±0.004) Ma.

5.3. Chronostratigraphic comparison with other records

The sequence of biostratigraphic and magnetostratigraphic events found in Gorrondatxe is apt for comparison with the results obtained in other studies (Fig. 3; Table 2). Franceschi et al. (2015) and Francescone et al. (2019) calculated the astronomically calibrated age of the C21r/C21n chron reversal in Smirra (Italy) to be 47.59 and 47.76 Ma, respectively (Fig. 10). The latter age was subsequently adopted by Vandenberghe et al. (2016). Similar astronomically tuned ages of 47.83, 47.834 (±0.072) and 47.857 (±0.079) Ma were also calculated by Boulila et al. (2018) and Westerhold et al. (2017, 2020, their table S22), respectively, using data from IODP Site U1410 and ODP Site 1258. In Gorrondatxe, the inconclusive magnetostratigraphic interval between chrons C21r and C21n is estimated to extend from 48.073 (±0.004) to 47.968 (±0.004) Ma. The latter, being closer to the age obtained in previous studies for the C21r/C21n chron boundary, is more likely to represent the true magnetic reversal. This would support the above-mentioned interpretation that the inconclusive magnetic interval was affected by processes of delayed magnetization.

The astronomical tuning of the Gorrondatxe section also allowed

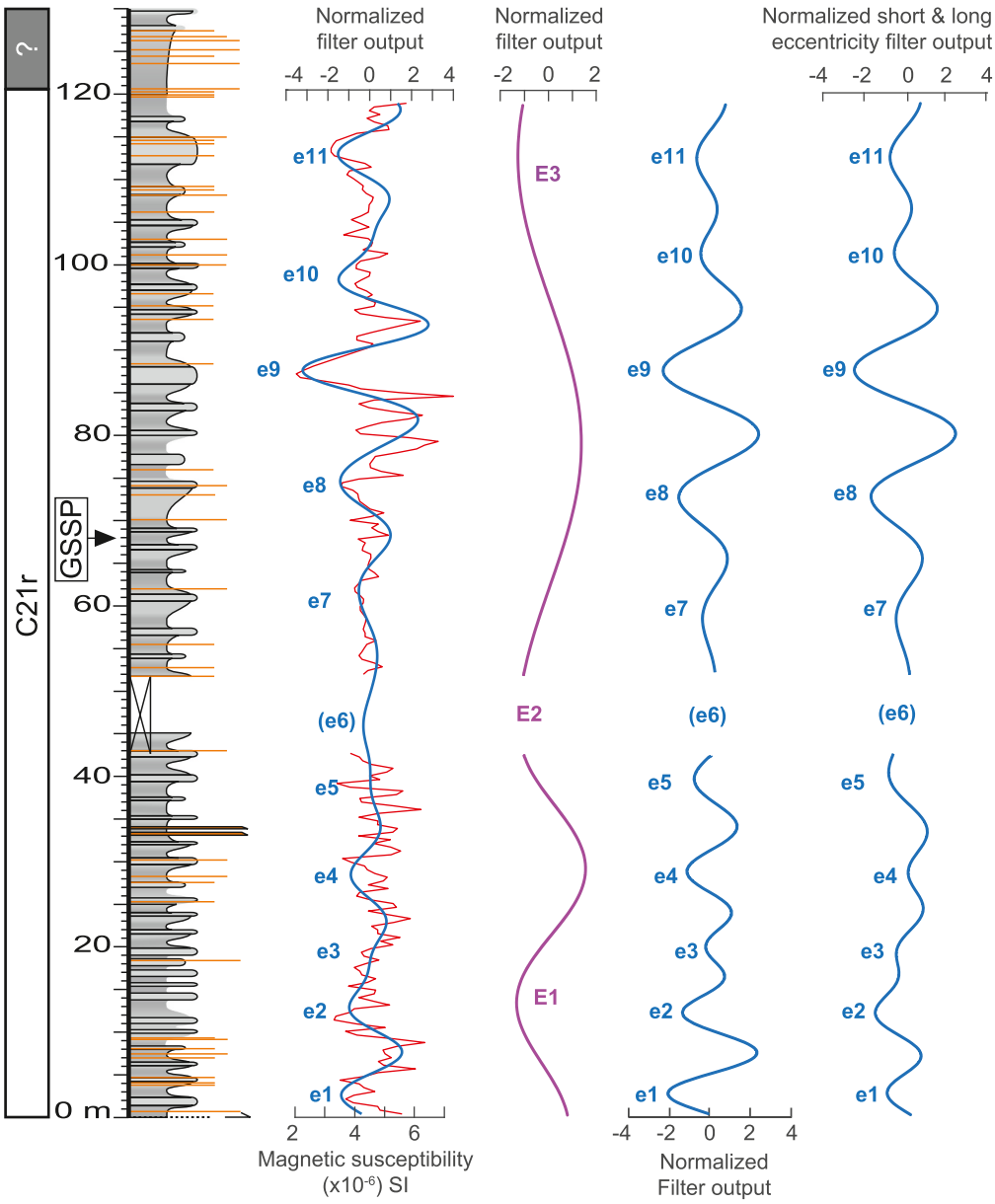

Fig. 8. Gaussian bandpass filter outputs of the Gorrondatxe bulk low-field mass magnetic susceptibility data series (red curve). The blue filter output on the left-hand graph (bandpass frequency 0.0925 ± 0.0625) shows 11 short eccentricity cycles (e1 to e11). Long-eccentricity (purple) filter outputs of the lower and upper parts of the Gorrondatxe section (bandpass frequencies 0.0265 ± 0.0115 and 0.0156 ± 0.0031, respectively), along with their short-eccentricity (blue) cycles (bandpass frequencies 0.096 ± 0.049 and 0.061 ± 0.0475, respectively) are also shown. The sum of both the long and short-eccentricity filter outputs is shown on the right-hand graph. (For interpretation of the references to colour in this figure legend, the reader is referred to the web version of this article.)

some biostratigraphic events to be age dated and compared with the ages obtained in previous studies, yielding variable results (Table 2). Notably, in Gorrondatxe the LO of *B. inflatus*, the GSSP marker event, can be astronomically tuned at 48.455 Ma. Both in Gorrondatxe (Bernaola et al., 2006; Molina et al., 2011) and Agost (southern Spain; Larrasoaña et al., 2008; Tori and Monechi, 2013) this biostratigraphic event was found within Chron C21r. On the contrary, several studies carried out in Newfoundland IODP Site U1410, Demerara Rise ODP Site 1258, and Smirra (Italy) found the LO of *B. inflatus* near the C21r/C21n chron reversal or within Chron C21n (Norris et al., 2014; Franceschi et al., 2015; Westerhold et al., 2017; Boulila et al., 2018; Cappelli et al., 2019). Finally, the LO of *B. inflatus* in ODP Site 1263 is problematic. Shipboard data reported this species from 226.21 (±0.03) rmcd (Zachos et al., 2004), which correlates with Chron C21r and was astronomically age dated at 48.427 (±0.002) by Westerhold et al. (2017, table S32; 2020, tables S18 and S21). This calibration is similar to that obtained in Gorrondatxe. However, Westerhold et al. (2017) could not replicate the original biostratigraphic data as *B. inflatus* was not found in their samples, rendering the biostratigraphy inconclusive (Fig. 10).

For the purposes of this study, attempting to clarify the biomagnetostratigraphic discrepancies was considered to be beyond its scope (see also Martínez-Braceras et al., 2023). However, several alternative scenarios can be put forward preliminarily, especially regarding the earlier LO of *B. inflatus* in Gorrondatxe. Firstly, some of the differences could be caused by paleocological factors, as *B. inflatus* were commonly thought to be rare or absent in true open ocean pelagic settings but more common in shallower hemipelagic settings (Westerhold et al., 2017; Cappelli et al., 2019). Secondly, the differences could also arise from taphonomic processes, as several studies showed that *rhabdoliths* in general and *Blackites* in particular were broadly distributed in Eocene neritic and oceanic settings, but only in exceptional (lagerstätte) sections do they show great abundance and good preservation (Bown, 2005; Bown & Newsam, 2017). These authors added that the scarcity of these taxa in many open marine sections is generally due to poor preservation. The fact that the record and preservation of *Blackites* in Gorrondatxe are exceptional could explain its apparently earlier occurrence. Finally, remagnetization processes similar to those identified in Gorrondatxe at the C21r/C21n chron transition could also have affected other sections. If this were the case in condensed oceanic records, the remagnetization could have extended into older deposits than in the

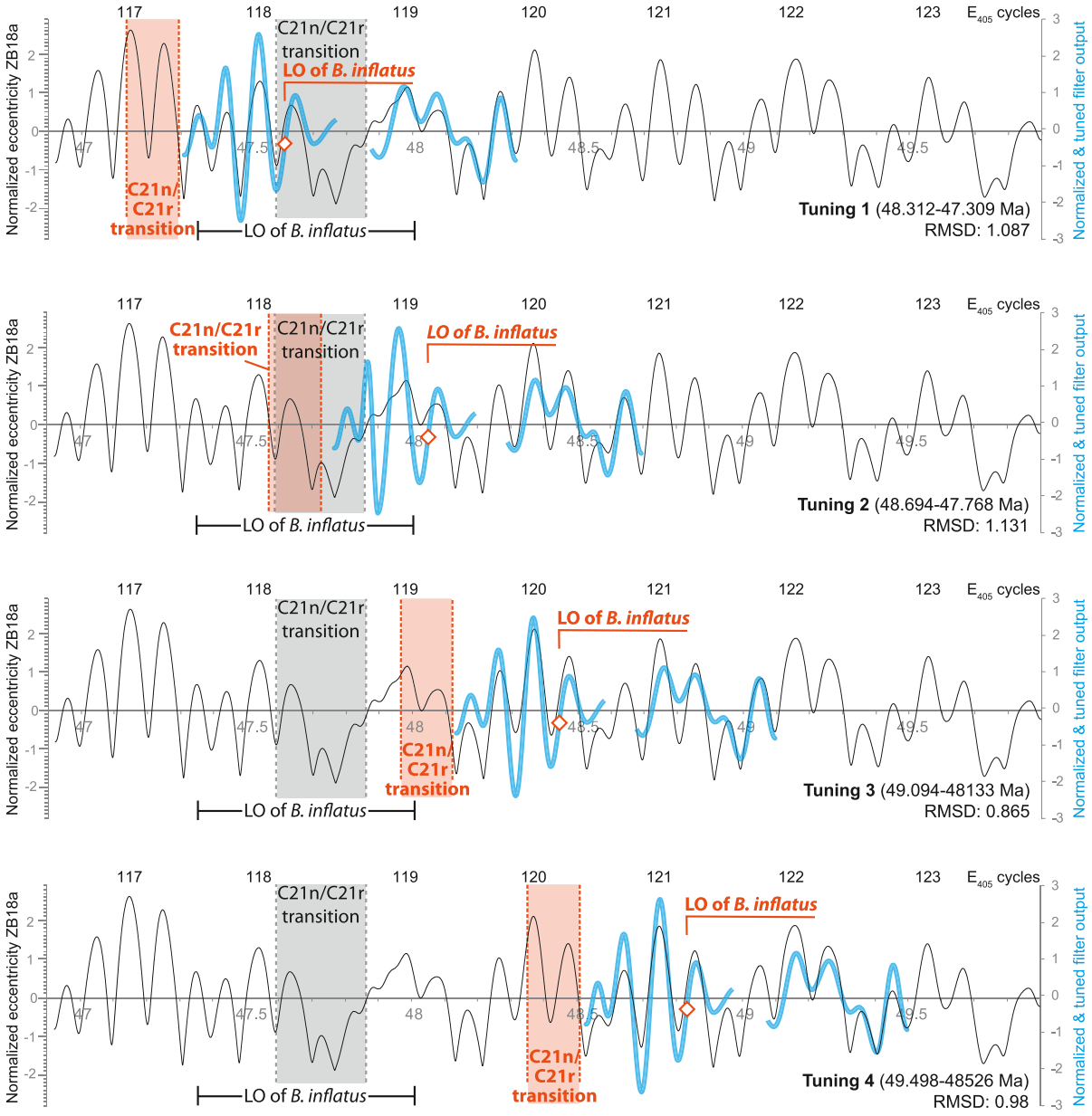

Fig. 9. Potential tuning of the combined long and short-eccentricity filter outputs from Gorrondatxe (blue curve) with different parts of the 46.9–49.9 Ma interval of the ZB18a orbital solution (black curve), which includes absolute 405-ky-long eccentricity cycles 117–123 (numbered from the Present). For comparison purposes, both data series were normalized. The red diamond in the Gorrondatxe filter outputs shows the position of the LO of *B. inflatus*, whereas the pale red area corresponds to the C21r/C21n Chron transition interval. The age ranges obtained in previous studies for the LO of *B. inflatus* and the C21r/C21n Chron boundary are shown by the horizontal black line and the grey area, respectively. Tuning option 3 is the chosen framework based on its lowest root-mean-square deviation (RMSD) from the orbital solution. (For interpretation of the references to colour in this figure legend, the reader is referred to the web version of this article.)

more expanded Gorrondatxe section, yielding apparently normal polarities around the LOs of *B. inflatus* and *N. cristata*. In any case, caution should be exercised when using problematic bioevents for comparison and correlation of different works and areas, pending clarification.

5.4. Suitability of the Lutetian GSSP

Despite some initial uncertainties about the position of the C21r/C21n chron boundary in Gorrondatxe, the cyclostratigraphic evidence suggests that this magnetic reversal can be located at 134.50 (±0.50) m and age dated at 47.968 (±0.004) Ma (Fig. 10; Table 2), which agrees with previous estimates (Franceschi et al., 2015; Francescone et al., 2019; Boulila et al., 2020; Speijer et al., 2020; Westerhold et al., 2020). The high diversity and good preservation of calcareous nannofossils, and the stratigraphic sequence of bioevents generally agreeing with the sequence found elsewhere (Fig. 3; Table 2), demonstrate that the Gorrondatxe biostratigraphic data are reliable, despite the differences in biomagnetostratigraphic calibration with other sections. Therefore, the Gorrondatxe section fulfils the requirements of a GSSP.

However, the comparison of several astronomically tuned successions strongly suggests that the marker event of the Lutetian GSSP at Gorrondatxe (i.e., the LO of *B. inflatus* at 67.85 m) is diachronous at a global scale (Fig. 10). While diachrony is not ideal for a GSSP marker event, it most likely affects many GSSPs marked by biostratigraphic events, especially by lowest and highest occurrences of species. In this regard, Remane et al. (1996, p.79) pointed out that chronostratigraphic boundaries should ideally be characterized by marker events of optimal correlation potential, but the potential diachrony of biostratigraphic

Table 2
Comparison of absolute ages (in Ma) assigned to significant events of the Ypresian/Lutetian transition in different studies.

Event	GTS2012 (Gradstein et al., 2012)	Smirra, Italy (Franceschi et al., 2015)	U1410 N Atlantic (Boulila et al., 2018)	U1410 N Atlantic (Cappelli et al., 2019)	GTS2020 (Gradstein et al., 2020)	1263, S Atlantic (Westerhold et al., 2020)	Gorrondatxe (this study)
LO *T. frontosa*	48.31	48.21					49.028 (Position derived from Payros et al., 2009; Molina et al., 2011)
HCO *D. lodoensis*	47.41 for HO		From 47.843 to older than 47.984			47.812 or 47.848 ± 0.045 for HO	48.841 ± 0.085
LO *B. praeinflatus*							48.717 ± 0.047
LO *B. pirjormis*	47.94						48.575 ± 0.002
LO *D. wemmelensis*		48.53					48.550 ± 0.003
LO *B. inflatus*	47.84	47.48	47.767 ± 0.057	47.35	48.07	48.427 ± 0.002 (Zachos et al., 2004)	48.455 ± 0.001
HCO *G. gammation*		47.76		47.26 for HO			48.435 ± 0.005
HO *B. pirjormis*	47.73						48.427 ± 0.005
LO *N. cristata*	47.73		Older than 47.984	47.26		47.523 ± 0.079 or 47.670 ± 0.051for *N.* Spp.	48.412 ± 0.005
HO *G. gammation*							48.162 ± 0.046
C21r/C21n	47.35	47.59	47.83		47.76	47.857 ± 0.079	47.968 ± 0.004

events does not necessarily make them unsuitable as primary markers of GSSPs. It should be taken into account that, once a GSSP is defined, the corresponding chronostratigraphic stage boundary is defined by the critical boundary level in the stratotype section, not by the marker event. In other words, the marker event does not determine the stage boundary, and other markers must therefore be available near the critical level in order to support chronostratigraphic correlation in sections other than the GSSP (Remane et al., 1996). Accordingly, the Ypresian/Lutetian boundary, as defined by the Gorrondatxe GSSP, corresponds to the 67.85 m stratigraphic layer of the section, which is marked by the LO of *B. inflatus*. The Ypresian/Lutetian boundary may not coincide with the LO of *B. inflatus* in other sections, but it should still be possible to identify this chronostratigraphic boundary using other secondary marker events (which, as reported in Molina et al., 2011, include planktonic and benthonic foraminifera, dinoflagellates, and other calcareous nannofossil bioevents, as well as magnetostratigraphic and sequence stratigraphic criteria). In this regard, the astronomically tuned cyclostratigraphy presented herein will contribute to increasing the correlation potential of the Gorrondatxe GSSP (Figs. 8 and 9). Furthermore, the cyclostratigraphic framework should also allow the correlation of the marine Gorrondatxe GSSP with terrestrial records (e.g. Zhang et al., 2021; Li et al., 2022), eventually enabling potential calibration with mammal and other continental biostratigraphic scales.

Steurbaut and Nolf (2021) argued against the use of the LO of *B. inflatus* in Gorrondatxe as the marker event for the Lutetian GSSP. They cited that *B. inflatus* is very rare in Eocene successions from the North Sea area, including the historical Lutetian stratotype in the Paris Basin. They also observed that this species is absent from reference lowermost Lutetian deposits in the North Sea area, and that some successions contain *Blackites praeinflatus*. They therefore concluded that the GSSP-based definition of the Lutetian Stage would mean that part of the referential Lutetian deposits of the historical stratotype area should be considered Ypresian in age, which they considered to be a *contradictio in terminis*. In order to address the anomaly, they suggested re-defining the Lutetian GSSP using the LO of *Discoaster sublodoensis* as a marker event, which they claimed to be approximately coeval with the LO of *B. praeinflatus*, the LCO of *Nannotetrina cristata*, and the HCO of *Discoaster lodoensis*. However, while their argument seems reasonable, they failed to take into account the following. Firstly, according to the GSSP concept of Remane et al. (1996), the base of the Lutetian stage is defined by the critical level in the Gorrondatxe section, not by the LO of *B. inflatus* marker event. Therefore, the fact that *B. inflatus* is rare in the North Sea area and that it only occurs at high stratigraphic levels of the historical Lutetian stratotype does not exclude the use of its LO as the marker event for the Lutetian GSSP elsewhere. Secondly, taking into account the abovementioned global diachrony in the LO of *B. inflatus*, it is very likely that this event is significantly younger in the North Sea area than in Gorrondatxe (Fig. 10). Consequently, the absence of *B. inflatus* in the lowermost deposits of the historical Lutetian stratotype does not imply that these deposits are older than the Lutetian GSSP in Gorrondatxe. Thirdly, the astronomically tuned age difference between the LOs of *B. praeinflatus* and *B. inflatus* is 262 (±47) ky (Table 2). This implies that the age of the deposits that contain *B. praeinflatus* in the historical Lutetian stratotype cannot be significantly older than the age of the Lutetian GSSP in Gorrondatxe; furthermore, the historical Lutetian stratotype deposits with *B. praeinflatus* could well be the same age, or even younger, than the Lutetian GSSP. These points mean that the Lutetian GSSP in Gorrondatxe does not necessarily result in a *contradictio in terminis* in the historical Lutetian stratotype. Additionally, the alternative marker events suggested by Steurbaut and Nolf (2021) for the Lutetian GSSP occur at different stratigraphic levels over a > 145.00-m thick interval in Gorrondatxe (Fig. 3), some predating and others postdating the LO of *B. inflatus*. This is probably a consequence of the condensed and/or discontinuous nature of the shallow-marine record of the North Sea sections, and the expanded and continuous record of the deep-marine Gorrondatxe section (Bernaola et al., 2006). Furthermore,

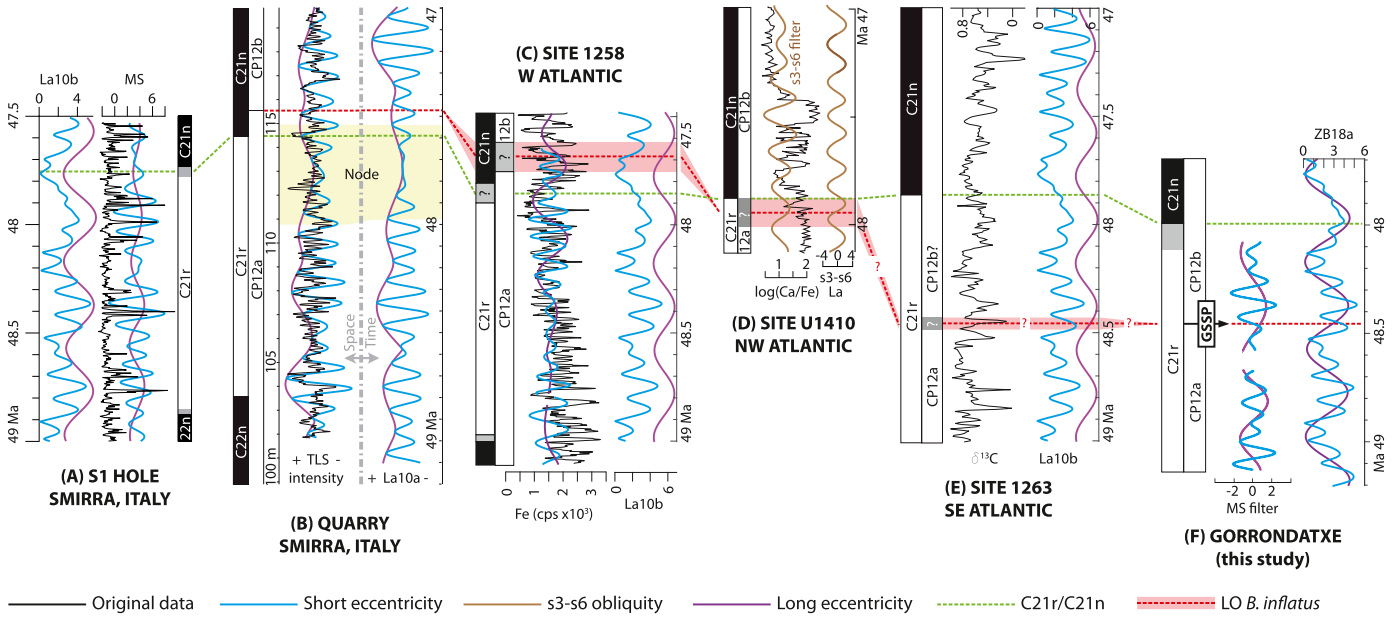

Fig. 10. Cyclochronological correlation of representative Ypresian/Lutetian successions, showing astronomically tuned ages of the C21r/C21n magnetic chron reversal (broken green line) and the lowest occurrence of *Blackites inflatus* (broken red line and/or pale red bands). La and ZB refer to orbital solutions used in the original studies for astronomical tuning (Laskar et al., 2011; Zeeben & Lourens, 2019). Blue curves represent short eccentricity cycles and purple curves show long eccentricity cycles; the brown curve in D represents the 173 ky-long s3-s6 obliquity modulation. (A) Magnetic susceptibility data (MS, SI units $x10^{-6}$) and cyclostratigraphy from hole S1 in Smirra, Italy (La10b eccentricity values $x10^{-2}$; Francescone et al., 2019). (B) Terrestrial laser scanner (TLS) imaging and cyclostratigraphy from the Smirra quarry (Franceschi et al., 2015). (C) Fe cps measurements and cyclostratigraphy from Demerara Rise (W equatorial Atlantic) Site 1258, correlated with La10b eccentricity cycles (values $x10^{-2}$) by Westerhold et al. (2009, 2017). (D) Site U1410 data series from Newfoundland, as astronomically tuned by Boulila et al. (2018) using 173 ky-long s3-s6 obliquity modulation (brown curves). (E) Benthic foraminifera $\delta^{13}C$ (‰) from Walvis Ridge Site 1263 (Loess smooth data series in table S34 of Westerhold et al., 2020; magnetostratigraphy from their table S22) and astronomical tuning (from their fig. S11; La10b eccentricity values $x10^{-2}$). Note that Zachos et al. (2004) pinpointed the base of Subzone CP12b but this bioevent could not be identified by Westerhold et al. (2017), rendering the biostratigraphy uncertain. (F) Astronomically tuned cyclostratigraphy from Gorrondatxe (this study) in the time domain (ZB18a eccentricity values $x10^{-2}$). (For interpretation of the references to colour in this figure legend, the reader is referred to the web version of this article.)

the main alternative marker event suggested by Steurbaut and Nolf (2021) for the Lutetian GSSP (i.e., the LO of *D. sublodoensis*) displays a discontinuous pattern and is therefore difficult to pinpoint. This difficulty is exacerbated by issues derived from the relatively long and morphologically complex transition between the ancestor species (i.e., *D. lodoensis*) and its offspring (i.e., *D. sublodoensis*), which result in subjective taxonomic interpretations. It should also be taken into account that the LO of *D. sublodoensis* occurs within the so-called Paniselian deposits in the North Sea area, which were originally included in the upper part of the historical Ypresian stratotype in Belgium (Molina et al., 2011). Therefore, using the LO of *D. sublodoensis* as marker event for the Ypresian/Lutetian boundary would imply that some of the historical Ypresian stratotype deposits should be considered Lutetian in age, a potential *contradictio in terminis* against the argument by Steurbaut and Nolf (2021).

In conclusion, the Gorrondatxe section offers a reliable astronomically tuned sequence of biomagnestostratigraphic events that provides a reference chronostratigraphic model of global significance, as expected of any GSSP. The LO of *B. inflatus* is the main marker event of the Lutetian GSSP level in Gorrondatxe, but many secondary markers identified both below and above the Ypresian/Lutetian boundary (Table 2; also see other events in Molina et al., 2011), as well as the cyclostratigraphy presented herein (Figs. 8 and 9), can help to approximate the boundary level in sections in which the main marker event cannot be identified or is unreliable. In this regard, the available evidence suggests that the Lutetian GSSP level in Gorrondatxe is a globally significant reference level that preserves the integrity of the historical Ypresian and Lutetian stratoypes of the North Sea area.

6. Conclusions

The validity of the GSSP for the base of the Lutetian Stage, defined by the LO of *B. inflatus* at the Gorrondatxe section, was put in doubt by several subsequent studies carried out in other areas. However, the further study of Ypresian/Lutetian succession of the Gorrondatxe section shows that the chronostratigraphic framework derived from Gorrondatxe is reliable. Furthermore, the cyclostratigraphic analysis carried out herein has provided astronomically tuned ages of biomagnetostratigraphic events that, in many cases, compare well with those from other studies. One exception is the LO of *B. inflatus*, which seems to be older in Gorrondatxe than in the Atlantic (Newfoundland, Demerara Rise) and Mediterranean (Italian) areas (Fig. 10). This delayed LO of *B. inflatus* was most likely driven by preservation issues in purely pelagic settings and probably also affected the shallow-marine historical reference sections of the North Sea area. However, the diachrony of the LO of *B. inflatus* should not affect the validity of the Lutetian GSSP in Gorrondatxe, as the chronostratigraphic stage boundary is defined by the critical level in the stratotype section, not by its marker event. Other secondary marker events identified in Gorrondatxe around the Lutetian GSSP, as well as the astronomically tuned cyclostratigraphic framework presented herein, can help to identify the chronostratigraphic stage boundary in sections in which the use of the primary marker event is not viable. Accordingly, the *contradictio in terminis* alluded by some authors (i.e., that the use of the LO of *B. inflatus* as the marker for the Lutetian GSSP caused some historical Lutetian sections of the North Sea area to be considered Ypresian in age) has no basis. In fact, this study further shows that the definition of the base of the Lutetian Stage by the Gorrondatxe GSSP best guarantees that the original concepts of both the Ypresian and Lutetian historical stratotypes are maintained. Other potential marker events for the GSSP-based Lutetian Stage would either alter the top of

the historical Ypresian stratotype (this would be the case of the LO of *D. sublodoensis* recently suggested as an alternative marker by some authors) or could affect the lowermost deposits of the historical Lutetian stratotype. In conclusion, the GSSP for the base of the Lutetian Stage at 67.85 m of the Gorrondatxe section, marked by the LO of *B. inflatus* and now astronomically age dated at 48.455 Ma, provides the most reliable chronostratigraphic model available to date, despite the diachrony of its marker event at a global scale.

Declaration of Competing Interest

The authors declare the following financial interests/personal relationships which may be considered as potential competing interests:

Aitor Payros reports financial support was provided by Spanish Foundation for Science and Technology. Aitor Payros reports financial support was provided by Basque Government.

Data availability

Data available as supplementary material

Acknowledgements

Research funded by projects PID2019-105670GB-I00/AEI/10.13039/501100011033 and UKRIA4D (PID2019-104693GB-I00/CTA) of the Spanish Government (MCIN/AEI) and by the Consolidated Research Group IT602-22 of the Basque Government. NM-B is grateful for post-doctoral specialization grants DOCREC19/35 and ESPDOC21/49 from the University of the Basque Country (UPV/EHU) and a Margarita Salas contract (MARSA22/05) of the Spanish Government with Next Generation funds from the European Union. Thanks are due to Carl Sheaver for his language corrections and to two reviewers (J. Ogg and anonymous) for their comments on a previous version of the manuscript.

Appendix A. Supplementary data

Supplementary data to this article can be found online at https://doi.org/10.1016/j.palaeo.2023.111669.

References

Agnini, C., Fornaciari, E., Raffi, I., Catanzariti, R., Pälike, H., Backman, J., Rio, D., 2014. Biozonation and biochronology of Paleogene calcareous nannofossils from low and middle latitudes. Newslett. Strat. 47, 131–181.

Batenburg, S.J., Sprovieri, M., Gale, A.S., Hilgen, F.J., Hüsing, S., Laskar, J., Liebrand, D., Lirer, F., Orue-Etxebarria, X., Pelosi, N., Smit, J., 2012. Cyclostratigraphy and astronomical tuning of the late Maastrichtian at Zumaia (Basque Country, Northern Spain). Earth Planet. Sci. Lett. 359, 264–278.

Batenburg, S.J., Gale, A.S., Sprovieri, M., Hilgen, F.J., Thibault, N., Boussaha, M., Orue-Etxebarria, X., 2014. An astronomical time scale for the Maastrichtian based on the Zumaia and Sopelana sections (Basque Country, northern Spain). J. Geol. Soc. 171, 165–180.

Bernaola, G., Orue-Etxebarria, X., Payros, A., Dinarès-Turell, J., Tosquella, J., Apellaniz, E., Caballero, F., 2006. Biomagnetostratigraphic analysis of the Gorrondatxe section (Basque Country, western Pyrenees): its significance for the definition of the Ypresian/Lutetian boundary stratotype. Neues Jahrb. Geol. Palaontol. Abh. 241, 67–109.

Bosmans, J.H.C., Hilgen, F.J., Tuenter, E., Lourens, L.J., 2015. Obliquity forcing of low-latitude climate. Clim. Past 11, 1335–1346.

Boulila, S., Vahlenkamp, M., De Vleeschouwer, D., Laskar, J., Yamamoto, Y., Palïke, H., Kirtland-Turner, S., Sexton, P.F., Westerhold, T., Röhl, U., 2018. Towards a robust and consistent middle Eocene astronomical timesale. Earth Sci. Planet. Lett. 486, 94–107.

Cappelli, C., Bown, P.R., Westerhold, T., Bohaty, S.M., de Riu, M., Lobba, V., Yamamoto, Y., Agnini, C., 2019. The early to middle Eocene transition: an integrated calcareous nannofossil and stable isotope record from the Northwest Atlantic Ocean (Integrated Ocean Drilling Program Site U1410). Paleoceanogr. Paleoclim. 34, 1913–1930.

Dinarès-Turell, J., Dekkers, M., 1999. Inferred multistage diagenetic pathway for the Early Pliocene Trubi marls at Punta di Maiata (southern Sicily): paleomagnetic and rock-magnetic observations. In: Tarling, D.H., Turner, P. (Eds.), Palaeomagnetism and Diagenesis in Sediments, 15. Geol. Soc. London, Spec. Pub, pp. 53–69.

Dinarès-Turell, J., Baceta, J., Pujalte, V., Orue-Etxebarria, X., Bernaola, G., 2002. Magnetostratigraphic and cyclostratigraphic calibration of a prospective Palaeocene/Eocene stratotype at Zumaia (Basque Basin, northern Spain). Terra Nova 14, 371–378.

Dinarès-Turell, J., Baceta, J.I., Pujalte, V., Orue-Etxebarria, X., Bernaola, G., Lorito, S., 2003. Untangling the Palaeocene climatic rhythm: an astronomically calibrated early Palaeocene magnetostratigraphy and biostratigraphy at Zumaia (Basque basin, northern Spain). Earth Planet. Sci. Lett. 216, 483–500.

Dinarès-Turell, J., Baceta, J.I., Bernaola, G., Orue-Etxebarria, X., Pujalte, V., 2007. Closing the Mid-Paleocene gap: toward a complete astronomically tuned Paleocene Epoch and Selandian and Thanetian GSSPs at Zumaia (Basque Basin, W Pyrenees). Earth Planet. Sci. Lett. 262, 450–467.

Dinarès-Turell, J., Stoykova, K., Baceta, J.I., Ivanov, M., Pujalte, V., 2010. High-resolution intra- and interbasinal correlation of the Danian-Selandian transition (Early Paleocene): the Bjala section (Bulgaria) and the Selandian GSSP at Zumaia (Spain). Palaeogeogr. Palaeoclimatol. Palaeocol. 297, 511–533.

Dinarès-Turell, J., Pujalte, V., Stoykova, K., Baceta, J.I., Ivanov, M., 2012. The Palaeocene "top chron C27n" transient greenhouse episode: evidence from marine pelagic Atlantic and peri-Tethyan sections. Terra Nova 24, 477–486.

Dinarès-Turell, J., Westerhold, T., Pujalte, V., Röhl, U., Kroon, D., 2014. Astronomical calibration of the Danian stage (Early Paleocene) revisited: Settling chronologies of sedimentary records across the Atlantic and Pacific Oceans. Earth Planet. Sci. Lett. 405, 119–131.

Franceschi, M., Penasa, L., Coccioni, R., Gattacceca, J., Smit, J., Cascella, A., Mariani, S., Montanari, A., 2015. Terrestrial Laser Scanner imaging for the cyclostratigraphy and astronomical tuning of the Ypresian-Lutetian pelagic section of Smirra (Umbria-Marche Basin, Italy). Palaeogeogr. Palaeoclim. Palaeoecol. 440, 33–46.

Francescone, F., Lauretano, V., Bouligand, C., Moretti, M., Sabatino, N., Schrader, C., Catanzariti, R., Hilgen, F., Lanci, L., Antonio Turtù, A., Sprovieri, M., Lourens, L., Galeotti, S., 2019. A 9 million-year-long astrochronological record of the early–middle Eocene corroborated by seafloor spreading rates. GSA Bull. 131, 499–520.

Hilgen, F.J., Kuiper, K.F., Lourens, L.J., 2010. Evaluation of the astronomical time scale for the Paleocene and earliest Eocene. Earth Planet. Sci. Lett. 300, 19–151.

Hinnov, L.A., 2013. Cyclostratigraphy and its revolutionizing applications in the earth and planetary sciences. GSA Bull. 125, 1703–1734.

Intxauspe-Zubiaurre, B., Payros, A., Flores, J.A., Apellaniz, E., 2017a. Changes to sea-surface characteristics during the middle Eocene (47.4 Ma) C21r–H6 event: evidence from calcareous nannofossil assemblages of the Gorrondatxe section (western Pyrenees). Newslett. Strat. 50, 245–267.

Intxauspe-Zubiaurre, B., Flores, J.A., Payros, A., 2017b. Variations to calcareous nannofossil CaCO3 content during the middle Eocene C21r–H6 hyperthermal event (~47.4 Ma) in the Gorrondatxe section (Bay of Biscay, western Pyrenees). Palaeogeogr. Palaeoclim. Palaeoecol. 487, 296–306.

Kirschvink, J.L., 1980. The least-squares line and plane and the analysis of palaeomagnetic data. Geophys. J. R. Astronom. Soc. 62, 699–718.

Kodama, K.P., Hinnov, L.A., 2015. In: Rock Magnetic Cyclostratigraphy. Wiley Blackwell, West Sussex, p. 165.

Larrasoaña, J.C., Gonzalvo, C., Molina, E., Monechi, S., Ortiz, S., Tori, F., Tosquella, J., 2008. Integrated magnetobiochronology of the Early/Middle Eocene transition at Agost (Spain): implications for defining the Ypresian/Lutetian boundary stratotype. Lethaia 41, 395–415.

Laskar, J., 2020. Astrochronology. In: Gradstein, F.M., Ogg, J.G., Schmitz, M.D., Ogg, G. M. (Eds.), Geologic Times Scale 2020. Elsevier, Amsterdam, pp. 139–158.

Laskar, J., Robutel, P., Joutel, F., Gastineau, M., Correia, A.C.M., Levrard, B., 2004. A long-term numerical solution for the insolation quantities of the Earth. Astron. Astrophys. 428, 261–285.

Laskar, J., Fienga, A., Gastineau, M., Manche, H., 2011a. La2010 a new orbital solution for the long-term motion of the Earth. Astron. Astrophys. 532, A89.

Li, M.S., Hinnov, L., Kump, L., 2019. Acycle: time-series analysis software for paleoclimate research and education. Comput. Geosci. 127, 12–22.

Li, Y., Sun, P., Liu, Z., Bai, Y., Xu, Y., Ma, L., Liu, R., 2022. Eocene hyperthermal events in the terrestrial system: geochronological and astrochronological constraints in the Fushun Basin, NE China. Mar. Petr. Geol. 139, 105604.

Luterbacher, H.P., Ali, J.R., Brinkhuis, H., Gradstein, F.M., Hooker, J.J., Monechi, S., Ogg, J.G., Powell, J., Röhl, U., Sanfilipo, A., Schmitz, B., 2004. The Paleogene Period. In: Gradstein, F.M., Ogg, J.G., Smith, A.G. (Eds.), A Geologic Time Scale 2004. Cambridge University Press, Cambridge, pp. 384–408.

Mann, M.E., Lees, J.M., 1996. Robust estimation of background noise and signal detection in climatic time series. Clim. Chang. 33, 409–445.

Martínez-Braceras, N., Payros, A., Miniati, F., Arostegi, J., Franceschetti, G., 2017. Contrasting environmental effects of astronomically driven climate change on three Eocene hemipelagic successions from the Basque-Cantabrian Basin. Sedimentology 64, 960–986.

Martínez-Braceras, N., Payros, A., Arostegi, J., Dinarès-Turell, J., 2021. Physical and geochemical record of an early Eocene carbon-cycle perturbation on a turbiditic continental margin. Sedimentology 68, 881–904.

Martínez-Braceras, N., Franceschetti, G., Payros, A., Monechi, S., Dinarès-Turell, J., 2023. High-resolution cyclochronology of the lowermost Ypresian Arnakatxa section (Basque-Cantabrian Basin, western Pyrenees). Newslett. Strat. 56, 53–74.

Meyers, S.R., 2012. Seeing red in cyclic stratigraphy: spectral noise estimation for astrochronology. Paleoceanography 27, PA3228.

Meyers, S.R., 2014. Astrochron: An R Package for Astrochronology, 0.6 Edition.

Molina, E., Alegret, L., Apellaniz, E., Bernaola, G., Caballero, F., Dinarès-Turell, J., Hardenbol, J., Heilmann-Clausen, C., Larrasoaña, J.C., Luterbacher, H., Monechi, S., Ortiz, S., Orue-Etxebarria, X., Payros, A., Pujalte, V., Rodríguez-Tovar, F.J., Tori, F.,

Tosquella, J., Uchman, A., 2011. The Global Stratotype Section and Point (GSSP) for the base of the Lutetian Stage at the Gorrondatxe section, Spain. Episodes 34, 86–108.
Norris, R.D., Wilson, P.A., Blum, P., Fehr, A., Agnini, C., Bornemann, A., Boulila, S., Bown, P.R., Cournede, C., Friederich, O., Ghosh, A.K., Hollis, C.J., Hull, P.M., Jo, K., Liu, Z., Matsui, H., Moriya, K., Nishi, H., Opdyke, B., Penman, D., Romans, B., Scher, H.D., Sexton, P., Takagi, H., Whiteside, J.H., Yamaguchi, T., Yamamoto, Y., 2014. Site U1410. In: Norris, R.D., Wilson, P.A., Blum, P. (Eds.), Paleogene Newfoundland Sediment Drifts. Proceed. IODP 342, College Station, TX, pp. 1–87.
Okada, H., Bukry, D., 1980. Supplementary modification and introduction of code numbers of the low-latitude coccolith biostratigraphic zonation (Bukry, 1973; 1975). Mar. Micropaleontol. 5, 321–325.
Payros, A., Martínez-Braceras, N., 2014. Orbital forcing in turbidite accumulation during the Eocene greenhouse interval. Sedimentology 61, 1411–1432.
Payros, A., Pujalte, V., 2020. Eocene mass-transport deposits in the Basque Basin (western Pyrenees, Spain): insights into mass-flow transformation and bulldozing processes. In: Ogata, K., Festa, A., Pini, G.A. (Eds.), Submarine Landslides: Subaqueous Mass Transport Deposits from Outcrops to Seismic Profiles, 246. AGU Geophys. Monogr, pp. 155–170.
Payros, A., Orue-Etxebarria, X., Pujalte, V., 2006. Covarying sedimentary and biotic fluctuations in Lower-Middle Eocene Pyrenean deep-sea deposits: Palaeoenvironmental implications. Palaeogeogr. Palaeoclim. Palaeoecol. 234, 258–276.
Payros, A., Bernaola, G., Orue-Etxebarria, X., Dinarès-Turell, J., Tosquella, J., Apellaniz, E., 2007. Reassessment of the Early-Middle Eocene biomagnetochronology based on evidence from the Gorrondatxe section (Basque Country, W Pyrenees). Lethaia 40, 183–195.
Payros, A., Orue-Etxebarria, X., Bernaola, G., Apellaniz, E., Dinarès-Turell, J., Tosquella, J., Caballero, F., 2009. Characterization and astronomically calibrated age of the first occurrence of Turborotalia frontosa in the Gorrondatxe section, a prospective Lutetian GSSP: implications for the Eocene time scale. Lethaia 42, 255–264.
Payros, A., Dinarès-Turell, J., Bernaola, G., Orue-Etxebarria, X., Apellaniz, E., Tosquella, J., 2011. On the age of the Early/Middle Eocene boundary and other related events: cyclostratigraphic refinements from the Pyrenean Otsakar section and the Lutetian GSSP. Geol. Mag. 148, 442–460.
Payros, A., Ortiz, S., Alegret, L., Orue-Etxebarria, X., Apellaniz, E., Molina, E., 2012. An early Lutetian carbon-cycle perturbation: Insights from the Gorrondatxe section (western Pyrenees, Bay of Biscay). Paleoceanography 27, PA2213.
Payros, A., Ortiz, S., Millán, I., Arostegi, J., Orue-Etxebarria, X., Apellaniz, E., 2015. Early Eocene climatic optimum: Environmental impact on the North Iberian continental margin. GSA Bull. 127, 1632–1644.
Remane, J., Bassett, M.G., Cowie, J.W., Gohrbandt, K.H., Lane, H.R., Michelsen, O., Naiwen, W., 1996. Revised guidelines for the establishment of global chronostratigraphic standards by the International Commission on Stratigraphy (ICS). Episodes 19, 77–81.
Roberts, A.P., Winklhofer, M., 2004. Why are geomagnetic excursions not always recorded in sediments? Constraints from post-depositional remanent magnetization lock-in modelling. Earth Planet. Sci. Lett. 227, 345–359.
Speijer, R.P., Pälike, H., Hollis, C.J., Hooker, J.J., Ogg, J.G., 2020. The Paleogene Period. In: Gradstein, F.M., Ogg, J.G., Schmitz, M.D., Ogg, G.M. (Eds.), Geologic Times Scale 2020. Elsevier, Amsterdam, pp. 1087–1140.
Steurbaut, E., Nolf, D., 2021. The Mont-des-Récollets section (N France): a key site for the Ypresian-Lutetian transition at mid-latitudes: reassessment of the boundary criterion for the base-Lutetian GSSP. Geodiversitas 43, 311–363.
Suganuma, Y., Yokoyama, Y., Yamazaki, T., Kawamura, K., Horng, C.S., Matsuzaki, H., 2010. 10Be evidence for delayed acquisition of remanent magnetization in marine sediments: implication for a new age for the Matuyama-Brunhes boundary. Earth Planet. Sci. Lett. 296, 443–450.
Thomson, D.J., 1982. Spectrum estimation and harmonic analysis. Proc. IEEE 70, 1055–1096.
Tori, F., Monechi, S., 2013. Lutetian calcareous nannofossil events in the Agost section (Spain): implications toward a revision of the Middle Eocene biomagnetostratigraphy. Lethaia 46, 293–307.
Torrence, C., Compo, G.P., 1998. A Practical Guide to Wavelet Analysis. Bull. Amer. Meteorol. Soc. 79, 61–78.
Vandenberghe, N., Hilger, F.J., Speijer, R.P., 2012. The Paleogene Period. In: Gradstein, F.M., Ogg, J.G., Schmitz, M.D., Ogg, G.M. (Eds.), The Geologic Time Scale 2012. Elsevier, Amsterdam, pp. 855–921.
Wade, B.S., Pearson, P.N., Berggren, W.A., Palike, H., 2011. Review and revision of Cenozoic tropical planktonic foraminiferal biostratigraphy and calibration to the geomagnetic polarity and astronomical time scale. Earth-Sci. Rev. 104, 111–142.
Weedon, G.P., 2003. In: Time-Series Analysis and Cyclostratigraphy: Examining Stratigraphic Records of Environmental Cycles. Cambridge University Press, Cambridge, p. 259.
Westerhold, T., Röhl, U., 2009. High resolution cyclostratigraphy of the early Eocene: new insights into the origin of the Cenozoic cooling trend. Clim. Past 5, 309–327.
Westerhold, T., Röhl, U., Frederichs, T., Bohaty, S., Zachos, J., 2015. Astronomical calibration of the geological timescale: closing the middle Eocene gap. Clim. Past 11, 1181–1195.
Westerhold, T., Röhl, U., Frederichs, T., Agnini, C., Raffi, I., Zachos, J.C., Wilkens, R.H., 2017. Astronomical calibration of the Ypresian timescale: implications for seafloor spreading rates and the chaotic behavior of the solar system? Clim. Past 13, 1129–1152.
Westerhold, T., Marwan, N., Drury, A.J., Liebrand, D., Agnini, C., Anagnostou, E., Barnet, J.S.K., Bohaty, S.M., De Vleeschouwer, D., Florindo, F., Frederichs, T., Hodell, D.A., Holbourn, A.E., Kroon, D., Lauretano, V., Littler, K., Lourens, L.J., Lyle, M., Pälike, H., Röhl, U., Tian, J., Wilkens, R.H., Wilson, P.A., Zachos, J.C., 2020. An astronomically dated record of Earth's climate and its predictability over the last 66 million years. Science 369, 1383–1387.
Zachos, J.C., Kroon, D., Blum, P., 2004. Early Cenozoic extreme climates: the Walvis Ridge transect. In: Proc. ODP, Init. Rep. 208. College Station, TX. https://doi.org/10.2973/odp.proc.ir.208.2004.
Zeebe, R.E., Lourens, L.J., 2019. Solar System chaos and the Paleocene-Eocene boundary age constrained by geology and astronomy. Science 365, 926–929.
Zhang, R., Kravchinsky, V.A., Qin, J., Goguitchaichvili, A., Li, J., 2021. One and a half million yearlong aridity during the middle Eocene in North-West China linked to a global cooling episode. J. Geophys. Res. Sol. Earth 126, e2020JB021037.
Zijderveld, J.D.A., 1967. AC demagnetisation of rock: analysis of results. In: Collinson, D. W., et al. (Eds.), Methods in Palaeomagnetism. Elsevier, Amsterdam, pp. 254–286.